# INTEGRATED ELECTRONIC AND OPTOELECTRONIC CIRCUITS AND DEVICES FOR PULSED TIME-OF-FLIGHT LASER RANGEFINDING

***PASI PALOJÄRVI***

Department of Electrical and Information Engineering and Infotech Oulu, University of Oulu

OULU 2003

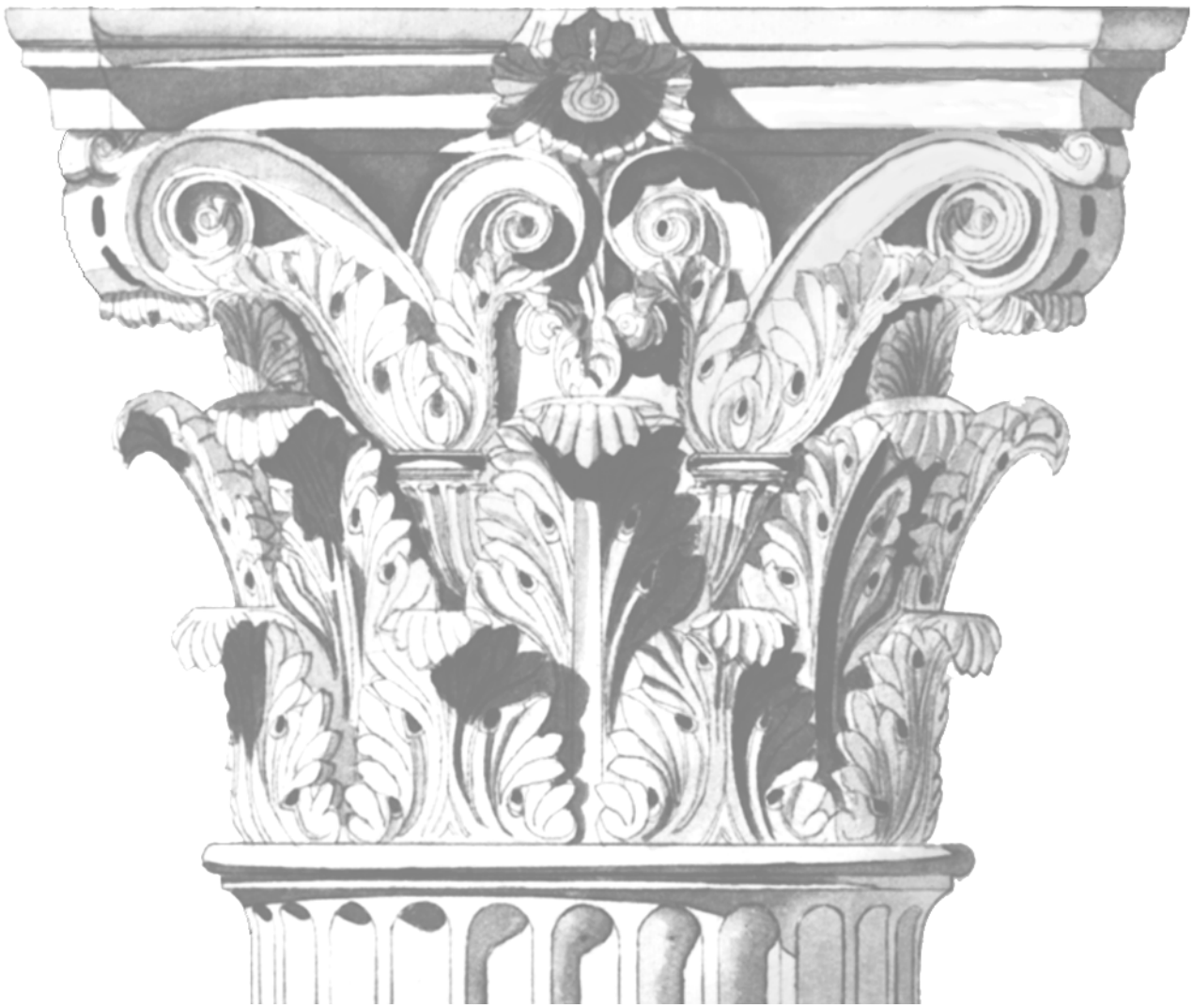

*PASI PALOJÄRVI*

# INTEGRATED ELECTRONIC AND OPTOELECTRONIC CIRCUITS AND DEVICES FOR PULSED TIME-OF-FLIGHT LASER RANGEFINDING

Academic Dissertation to be presented with the assent of the Faculty of Technology, University of Oulu, for public discussion in Raahensali (Auditorium L10), Linnanmaa, on April 4th, 2003, at 12 noon.

OULUN YLIOPISTO, OULU 2003

Reviewed by
Professor Günter Kompa
Professor Hannu Tenhunen

ISBN 951-42-6966-7 (URL: http://herkules.oulu.fi/isbn9514269667/)

ALSO AVAILABLE IN PRINTED FORMAT
Acta Univ. Oul. C 181, 2003
ISBN 951-42-6965-9
ISSN 0355-3213 (URL: http://herkules.oulu.fi/issn03553213/)

OULU UNIVERSITY PRESS
OULU 2003

**Palojärvi, Pasi, Integrated electronic and optoelectronic circuits and devices for pulsed time-of-flight laser rangefinding**
Department of Electrical and Information Engineering and Infotech Oulu, University of Oulu, P.O.Box 4500, FIN-90014 University of Oulu, Finland
Oulu, Finland
2003

***Abstract***

The main focus of this work concerned with the development of integrated electronic and optoelectronic circuits and devices for pulsed time-of-flight laser rangefinding is on the construction of the receiver channel, system level integration aimed at realisation of the laser radar module and in integration of all the receiver functions of laser radar on one chip.

Since the timing discriminator is a very important part of a pulsed time-of-flight laser rangefinder, two timing discrimination methods are presented and verified by means of circuit implementations, a leading edge discriminator and a high-pass timing discriminator. The walk error of the high-pass timing discriminator is ±4 mm in a dynamic range of 1:620 and the uncompensatable walk error of the leading edge discriminator is ±30 mm in a dynamic range of 1:4000. Additionally a new way of combining the timing discriminator with time interval measurement is presented which achieves a walk error of ±0.5 mm in a dynamic range of 1:21.

The usability of the receiver channel chip is verified by constructing three prototypes of pulsed TOF laser radar module. The laser radar achieves mm-level accuracy in a measurement range from 4 m to 34 m with non-cooperative targets. This performance is similar to that of earlier realisations using discrete components or even better and has markedly reduced power consumption and size.

The integration level has been increased further by implementing a photodetector on the same chip as the rest of the receiver electronics. The responsivity of the photodetector is about 0.3 A/W at 850 nm wavelength and the noise of the receiver is reduced by a factor of about two relative to realisations using an external photodetector, because of the absence of parasitic capacitances and inductances caused by packages, PCB wiring, bond wires and ESD and I/O cell structures.

The functionality of a multi-channel pulsed TOF laser radar chip is demonstrated using the photodiode structure investigated here. The chip includes four photodetectors with receiver channels and a three-channel time-to-digital converter. The chip together with external optics and a laser pulse transmitter enables distances to be measured in three directions with a single optical pulse, thus showing the feasibility of implementing all the receiver functions of a pulsed time-of-flight imager on a single chip using a current semiconductor process.

*Keywords:* integrated photodiode, laser rangefinding, timing discrimination

# Acknowledgements

This thesis is based on research work carried out at the Electronics Laboratory of the Department of Electrical Engineering and Infotech Oulu, University of Oulu, during the years 1994–2002.

I wish to express my gratitude to Professor Juha Kostamovaara, who has supervised this work for his tireless encouragement and guidance. I am also grateful to Dr. Tarmo Ruotsalainen and Dr. Kari Määttä for their help and support. I thank my colleagues at the Electronics Laboratory for the pleasant working atmosphere and for their assistance. My family deserve my warmest thanks for their support during these years.

I wish to thank Professors Günter Kompa and Hannu Tenhunen for examining this thesis, and Mr. Malcolm Hicks for revising the English of the manuscript.

The work was supported financially by the Graduate School in Electronics, Telecommunications and Automation, the Academy of Finland, the Technology Development Centre of Finland (TEKES) and the foundations Emil Aaltosen säätiö, Oulun yliopiston tukisäätiö, Seppo Säynäjäkankaan tiedesäätiö, Tauno Tönningin säätiö, Tekniikan edistämissäätiö and Walter Ahlströmin säätiö, all of which are gratefully acknowledged.

Oulu, March 2003 Pasi Palojärvi

# List of terms, symbols and abbreviations

The terms describing the performance of the measurement equipment are defined according to the IEEE Standard Dictionary of Electrical and Electronics Terms (IEEE 1996):
**accuracy** is the degree of correctness with which a measured value agrees with the true value
**jitter** is the short-term deviations of the significant instants of a signal from their ideal positions in time
**precision** is the quality of coherence or repeatibility of measurement data, customarily expressed in terms of the standard deviation of the extendend set of measurement results
**resolution** is the least value of the measured quantity that can be distinguished

| | |
|---|---|
| A/D | analogue to digital |
| AlGaAs | aluminium gallium arsenide |
| AM | amplitude modulation |
| APD | avalanche photodiode |
| ARC | amplitude and rise time compensation |
| ASIC | application-specific integrated circuit |
| BiCMOS | bipolar-CMOS, a semiconductor process containing bipolar and CMOS transistors |
| CFD | constant fraction discriminator |
| CMGC | current mode gain control |
| CMOS | complementary MOS, a semiconductor process containing both NMOS and PMOS transistors |
| CR | capacitor-resistor |
| CW | continuous wave |
| EGC | electronic gain control |
| ESD | electrostatic discharge |
| FM | frequency modulation |
| FWHM | full width at half maximum |
| GaAs | gallium arsenide |
| IR | infrared |

| | |
|---|---|
| MOS | metal –oxide semiconductor |
| NIR | near-infrared |
| NMOS | n-channel MOS |
| PC | personal computer |
| PCB | printed circuit board |
| PIN | p-i-n photodiode |
| PMOS | p-channel MOS |
| PMT | photomultiplier tube |
| PSRR | power supply rejection ratio |
| RC | resistor-capacitor |
| rms | root mean square |
| SNR | signal to noise ratio, here the ratio of the peak signal voltage to the rms of the noise voltage |
| SOI | Silicon-on-Insulator |
| TAC | time-to-amplitude converter |
| TDC | time-to-digital converter |
| TOF | time of flight |
| VMGC | voltage mode gain control |

| | |
|---|---|
| A | voltage gain |
| $c$ | speed of light |
| $f_T$ | transit frequency |
| $I_b$ | bias current |
| $I_{out}$ | output current signal |
| $t_p$ | timing point |
| $t_r$ | rise time (from 10% to 90%) |
| $v_{in}$ | input voltage signal |
| $V_{max}$ | maximum amplitude |
| $v_p$ | peak amplitude |
| $V_{offset}$ | offset voltage |
| $v_{out}$ | output voltage signal |
| $V_{th}$ | threshold voltage |
| Z | transimpedance gain |

| | |
|---|---|
| $\sigma_t$ | standard deviation of the timing point |
| $\sigma_v$ | noise power |

# List of original papers

I Ruotsalainen T, Palojärvi P & Kostamovaara J (2001) A Wide Dynamic Range Receiver Channel for a Pulsed Time-of-Flight Laser Radar. IEEE Journal of Solid-State Circuits 36(8): 1228–1238.

II Peltola T, Ruotsalainen T, Palojärvi P & Kostamovaara J (2000) A Receiver Channel with a Leading Edge Timing Discriminator for a Pulsed Time-of-Flight Laser Radar. Proc. 26th European Solid-State Circuits Conference, Stockholm, Sweden, 428–431.

III Palojärvi P, Ruotsalainen T & Kostamovaara J (1999) A New Approach to Avoid Walk Error in Pulsed Laser Rangefinding. Proc. IEEE International Symposium on Circuits and Systems, Orlando, Florida, USA, 1: 258–261.

IV Palojärvi P, Määttä K & Kostamovaara J (1997) Integrated Time-of-flight Laser Radar. IEEE Transactions on Instrumentation & Measurement 46(4): 996–999.

V Palojärvi P, Määttä K & Kostamovaara J (1999) Pulsed Time-of-Flight Laser Radar Based on Custom Designed Receiver and Time Interval Measurement Ics. Proc. 2nd Topical Meeting on Optoelectronic Distance Measurements and Applications, Pavia, Italy, 299–304.

VI Palojärvi P, Määttä K & Kostamovaara J (2002) Pulsed Time-of-Flight Laser Radar Module with mm-level Accuracy Using Full Custom Receiver and TDC ASICs. IEEE Transactions on Instrumentation & Measurement 51(5): 1102–1108.

VII Palojärvi P, Ruotsalainen T & Kostamovaara J (2001) Pn Photodiodes for Pulsed Laser Rangefinding Applications Realized in Standard CMOS/BiCMOS Processes. Journal of Analog Integrated Circuits and Signal Processing, Kluwer Academic Publishers 27(3): 239–248.

VIII Palojärvi P, Ruotsalainen T & Kostamovaara J (1999) Integrated Optoelectronic Receiver for a Pulsed Time-of-Flight Laser Radar. Proc. 25th European Solid-State Circuits Conference, Duisburg, Germany, 294–297.

IX Palojärvi P, Mäntyniemi A & Kostamovaara J (2001) A Multi-channel Pulsed Time-of-Flight Laser Radar Chip. Proc. 3rd Topical Meeting on Optoelectronic Distance/Displacement Measurements and Applications, Pavia, Italy, 112–117.

The research work described in these original papers was carried out at the Electronics Laboratory, Department of Electrical Engineering, and Infotech Oulu, University of Oulu, Finland, during the years 1994–2002, in projects funded by the Academy of Finland, TEKES and several industrial companies. The projects were headed by Prof. Juha Kostamovaara, who also supervised this work.

Papers I to III describe receiver channel electronics for a pulsed TOF laser radar. The research described in paper I was done jointly by the author and T. Ruotsalainen, who prepared the manuscript, and that in paper II by the author, T. Ruotsalainen and T. Peltola, who prepared the manuscript. The circuit was developed during the research and has since been processed several times, the latest version being designed by the author.

Papers IV to VI describe pulsed TOF laser rangefinding devices. K. Määttä designed the PCB and the software for the controller of devices reported in papers V and VI and assisted in the measurements.

Paper VII describes photodiodes integrable in standard silicon technology. The work was done jointly by the author and T. Ruotsalainen.

Papers VIII and IX describe receivers for pulsed TOF laser radar devices in which integrated photodiodes are used. The three-channel time-to-digital converter was copied from a circuit designed by A. Mäntyniemi and then modified by the author so that it can measure three stop signals instead of one.

# Contents

# 1 Introduction

## 1.1 Previous work and aim of this research

Pulsed time-of-flight (TOF) laser rangefinding is one of the main areas of research at the Electronics Laboratory of the University of Oulu. Work began over twenty years ago (Ahola 1979), and 5 doctoral theses have been produced to date (Ahola 1987, Kostamovaara 1986, Määttä 1995, Ruotsalainen 1999a, Räisänen-Ruotsalainen 1998) together with numerous Licenciate theses and M.Sc. dissertations. The research has been concentrated in three subareas: receiver channel electronics, time interval measurement and generation of optical pulses, which together cover the main functions of a pulsed time-of-flight laser rangefinder. The ensuing co-operation has helped companies in the Oulu area to create and develop commercial products in the field of laser rangefinding.

The focus in the research at the Electronics Laboratory has moved from large, discrete component realisations into smaller realisations utilising full-custom application-specific integrated circuits (ASIC). The laser radars constructed using discrete components, shown in Fig. 1a, are already commercial products and achieve cm-level measurement accuracy with a power consumption of about 20 W (Määttä 1995). A prototype of a hand-held laser radar device, shown in Fig. 1b, that achieves mm-level accuracy with a power consumption 4 W (paper VI) utilises AISCs in the receiver channel and time interval measurement functions and is coupled to a portable PC for displaying and storing the results. The next phase in the research, which is already under way, is aimed at further increasing the level of integration and constructing a ”component-like” miniaturised laser radar which also includes a laser pulse transmitter. An example of the research is the receiver hybrid for a laser radar, comprising a photodetector, amplifier channel and timing discriminator, shown in Fig. 1c.


**Fig. 1. Three phases of laser radar research at the Electronics Laboratory.**

The aim of this work was to develop pulsed TOF laser rangefinding technologies for a laser radar module usable in industrial measurement applications where mm or cm-level accuracy is needed. The goal of this development effort was to reduce the size of the laser radar and to increase the level of integration. The smaller size would open up new applications such as positioning of tools and vehicles, anti-collision radars and proximity sensors.

## 1.2 Content and contributions of the work

The content of this thesis is as follows. The operating principle of the pulsed TOF laser rangefinder is described in Chapter 2. As the technique is based on measuring the time interval between transmitting and receiving an optical pulse, a logic level timing mark for the time-to-digital converter (TDC) has to be generated accurately from the pulse even when its amplitude varies. This is achieved with a timing discriminator, which is a critical block in a pulsed TOF laser radar from the performance point of view. Two ways of detecting the timing point from the pulse signal, a high-pass timing discriminator and a leading edge discriminator, are presented, together with their benefits and drawbacks. The origin of the walk error, a change in the timing mark when the amplitude of the signal changes, is also explained for both methods.

The development of pulsed TOF laser rangefinding techniques and structures suitable for a laser radar module is described in Chapter 3 with the aid of the original papers included at the end of the thesis. The chapter begins by presenting two integrated receiver channel realisations: the first with a high-pass timing discriminator (paper I) and the second with a leading edge discriminator (paper II). After that a new method for avoiding walk error by combining the timing discrimination and time interval measurement by means of linear signal processing is presented (paper III). The operation of the developed

integrated receiver channel is verified by constructing prototypes of a portable laser rangefinder, which are presented with their performance in papers IV–VI.

In order to further increase the level of integration and reduce the size and mechanical complexity of the laser radar, the possibility of integrating a photodetector into the same chip as the rest of the electronics was investigated. The properties of photodiodes implemented in standard CMOS/BiCMOS processes without any modifications were studied (paper VII), and finally two receiver chips with integrated photodiodes are described, one for "normal" distance measurement purposes (paper VIII) and the other for measuring distances from three separate targets with a single optical pulse. The latter chip includes four receiver channels with integrated photodetectors and a three-channel time-to-digital converter.

The results of the work are discussed and compared with research published in the literature in Chapter 4 and a summary of the work is given in Chapter 5.

The scientific contribution of the thesis lies in the development of integrated receiver channel realisations for a pulsed TOF laser radar and the construction of high-performance laser radar modules based on the use of these receivers. In this connection the origin of the walk error observed in the leading edge discriminator was also analysed. In addition, a totally new receiver channel structure based on combination of the timing discriminator with time interval measurement was developed and integration of the photodiode into the same chip as the rest of the receiver and the feasibility of an optoelectronic laser radar chip capable of measuring distances from three points with a single optical pulse were demonstrated.

# 2 Pulsed time-of-flight laser rangefinding

Laser rangefinders can be divided into several categories in terms of their operation principle. This work concentrates on a technique in which the distance is measured as a direct product of the propagation delay of a laser beam, i.e. the time-of-flight method, and still more precisely, in which a pulse wave is used as the laser beam, i.e. pulsed time-of-flight laser rangefinding.

Time-of-flight laser radars are used in wide variety of industrial, customer and military applications, including absolute distance measurements, profiling, automotive safety, vibration and proximity measurements, velocimetry, positioning, vehicle guidance and 3-D vision (Araki & Yoshida 1996, Kaisto *et al.* 1993, Kawashima *et al.* 1995, Määttä *et al.* 1993). Absence of physical contact and short measurement times with optically visible targets are distinguishing characteristics for all these types of measurement. Typical measurement distances are up to several ten metres, or even several kilometres in military applications in particular. The accuracy needed varies accordingly, from mm-level to a few metres. The most important performance parameters are precision, accuracy, measurement range and measurement time.

A pulsed time-of-flight laser rangefinding device typically consists of a laser pulse transmitter, the necessary optics, two receiver channels and a time-to-digital converter, as shown in Fig. 2. The laser pulse transmitter emits a short optical pulse (typically 2 to 20 ns) to an optically visible target and the transmission event is defined either optically, by detecting a fraction of the pulse, or electrically, from the drive signal of the laser diode. The start pulse is then processed in a receiver channel, which generates a logic-level start pulse for a TDC. In the same way the optical pulse reflected from the target and collected by the photodetector of the stop receiver channel is processed and a logic-level stop pulse is generated for the TDC. The TDC uses its time base to convert the time interval to a digital word which represents the distance from the target.

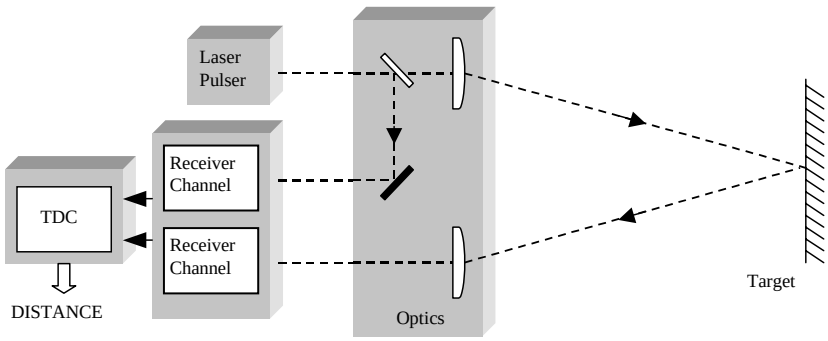


**Fig. 2. Principle of a pulsed time-of-flight laser rangefinder.**

The amplitude of the received stop signal varies over a wide range depending on the measurement distance and the reflectivity and angle of the target. The dynamic range of the signal depends on the application, and may be 1:1000 or even more. As the length of the laser beam is much longer than the accuracy usually needed (2 metres vs. a few millimetres or centimetres), a specific point in the pulse has to be defined, and consequently a logic-level pulse for the TDC has to be produced. The timing event should not change when the level of the signal varies, as it will directly affect the measurement result, with 6.7 ps corresponding to 1 mm.

The function of the receiver is to produce accurately timed logic-level pulses from optical input pulses of varying amplitude. Since the timing discriminator plays an important role in this process, solutions for this component are described in more detail here.

The timing event can be generated either from the edge of the pulse which is allowed to saturate in the receiver channel or by linear signal processing, in which gain control structures are usually needed, due to the wide dynamics of the input signal and the limited dynamic range of the receiver channel. The simplest way of defining the timing point is the former one, a leading edge discrimination technique in which a comparator with a constant threshold voltage is used to trigger the leading edge of the received pulse. The drawback of the technique is that if the amplitude of the pulse changes, the timing point also changes and generates a walk error $\Delta t$, as shown in Fig. 3a. Thus the walk error represents the change that takes place in the timing event when the amplitude of the pulse varies. The principle of operation of the leading edge timing discriminator and its walk error are presented in more detail in section 2.1.

In order to reduce the walk error, more sophisticated techniques has been developed in which the signal is processed in a linear manner. One technique of this kind is the well known constant fraction discriminator (CFD), where the timing point is generated by comparing an attenuated pulse and a delayed pulse, so that their crossing point defines a constant fraction of the pulse (Gedge & McDonald 1968). In this technique the timing point (crossing point) is insensitive to variation in the amplitude of the signal. If the shape of the rising edge does not vary, the method can be used for amplitude and rise time-compensated (ARC) timing, given proper selection of the delay (Paulus 1985). The CFD is well suited for applications in which the signal has a fast rising edge and a long tail (e.g. scintillation detector/PMT measurements in nuclear physics), because the

discriminator utilises only rising edge and peak amplitude information regarding the pulse. CFDs constructed with discrete components usually require delay lines, whereas an exact delay of a few nanoseconds is difficult to realise in integrated circuits without degradation in the slope and amplitude of the signal. The CFD is nevertheless integrable by means of operations such as attenuation, a C-R differentiator, an R-C low-pass filter or a distributed R-C delay line (Jackson *et al.* 1997).

A pulse signal which also has a fast falling edge (i.e. no long tail) can be generated using a PIN or APD as the photodetector. Here constant fraction detection can be implemented by identifying the crossing point between the falling edge of a pulse and the rising edge of a delayed pulse (Kostamovaara & Myllylä 1985). In integrated solutions, however, the technique again calls for an exact delay of some nanoseconds.

A simple C-R high-pass filter was used successfully here to discriminate the timing point of the pulse. This filter generates from the unipolar input pulse a bipolar output pulse in which the zero crossing point is insensitive to amplitude variations, as shown in Fig. 3b. The operation of the technique and the walk error originating from detection of the zero crossing point are presented in more detail in section 2.2.

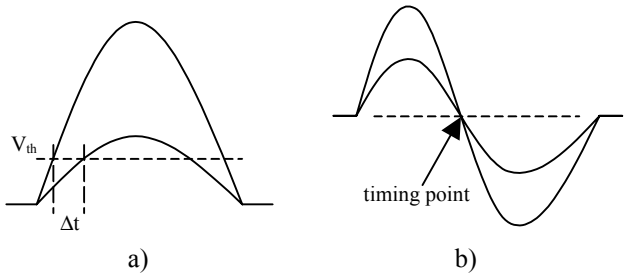


**Fig. 3. a) Walk error with a leading edge discriminator, and b) the bipolar pulse used in the high-pass timing discrimination technique.**

## 2.1 Leading edge discrimination

A leading edge discriminator is the simplest way to detect the arrival of a pulse. A comparator with a constant threshold voltage is used to define the timing mark for the TDC. The threshold voltage has to be so high that noise will not cause false triggerings. The walk error in the leading edge discrimination arises from the amplitude variation and shape of the input pulse, the bandwidth and dynamics of the receiver channel and the level of the threshold. The error consists of three sources: a geometrical timing error which occurs even with an ideal receiver, error caused by the finite bandwidth, slew-rate and dynamic range of the receiver and a change in the propagation delay of the timing comparator. The last-mentioned is usually negligible relative to the previous ones.

The walk error can be estimated by means of a simple piecewise linear model of the rising edge of the input pulse $V_{in}$, as shown in Fig. 4b, fed to an amplitude-limiting circuit

followed by a bandwidth limiting circuit, as shown in Fig. 4a (van de Plassche 1994). Using the notation in Fig. 4b, the delay in the timing point from the beginning of the rising edge $t_p$ at the output to the amplitude limiting circuit is

$$t_p = \frac{V_{th}}{v_p} \cdot t_r \,, \tag{1}$$

where $V_{th}$ is the threshold voltage and $v_p$ and $t_r$ are the peak amplitude and the rise time of the pulse before amplitude limitation. The delay variation represents the walk error of an ideal receiver channel (geometrical walk error). If, for example, the rise time of the pulse is 1.6 ns and the threshold is 50 mV, an amplitude variation from 100 mV to 2 V will results in a timing point variation from 0.8 ns to 40 ps and thus generate a walk error of 760 ps. In real applications, however, the maximum amplitude of the input pulse is much greater, so that the geometrical variation in the timing point in this case can be estimated to be 0.8 ns.

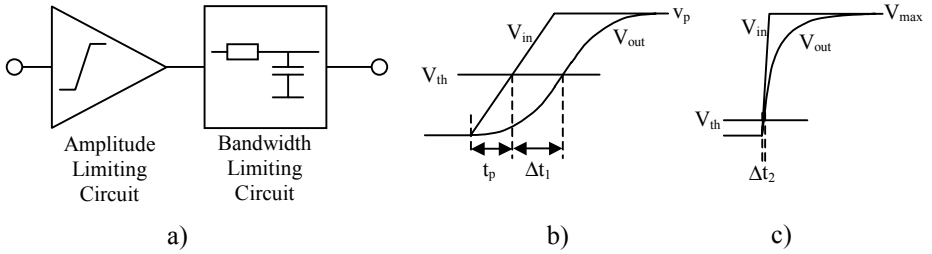


**Fig. 4. a) A simple model of the receiver channel and input and output signals of the bandwidth limiting circuit with b) small and c) large signal amplitudes.**

This model neglects slew-rate limitation and models the delay change caused by the finite bandwidth of the receiver by feeding the amplitude-limited signal into a single pole bandwidth limiting circuit. The largest input signal of the bandwidth limiting circuit can be estimated to be a step with an amplitude equal to the maximum linear amplitude of the amplifier channel $V_{max}$, as shown in Fig. 4c. This leads to an output signal waveform $v_{out}$ of

$$v_{out} = V_{\max}(1 - e^{-\frac{t}{RC}}) \,, \tag{2}$$

where $RC$ is the time constant of the bandwidth limiting circuit. The delay of the threshold crossing point, calculated using an $RC$ of 640 ps (corresponding to a bandwidth of 250 MHz), $V_{th}$ of 50 mV and $V_{max}$ of 2 V, is 16 ps, which represents the shortest delay. The longest delay appears with the smallest input signal, and if the slew rates of the input signal and the output signal of the bandwidth limiting circuit are equal at the threshold level, as shown in Fig. 4b, the delay is simply $RC$, corresponding to 640 ps. The bandwidth limitation thus generates a walk error of 624 ps, which is considerable in

relation to the walk error of 800 ps achieved with an ideal receiver channel (infinite bandwidth).

The walk error can be compensated for using a correction table in the range where the amplitude of the signal can be measured and the signal is not saturated. This calls for an accurate peak detector, because the compensation is very sensitive to amplitude changes at low signal levels (Ruotsalainen 1999a).

The walk error was simulated numerically using the Matlab program and the simulation model described above, but improved in the sense that the single pole of the bandwidth limiting circuit was replaced by three identical poles (a low-pass filter with a –60 dB/decade roll-off) so that the resulting –3 dB frequency was equal to 250 MHz. The delay in the timing point as a function of the input signal level is shown in Fig. 5. The curves show the geometrical walk error, the error caused by the finite bandwidth and the sum of these. The x-axis shows the ratio between the peak amplitude of the signal and the threshold level. The rise time of the input signal is assumed to be 1.6 ns and the maximum linear amplitude to be 40 times the threshold level (corresponding to $V_{th}$=50 mV and $V_{max}$=2 V), which means that the signal begins to saturate in the receiver after a value of 40 on the x-axis.

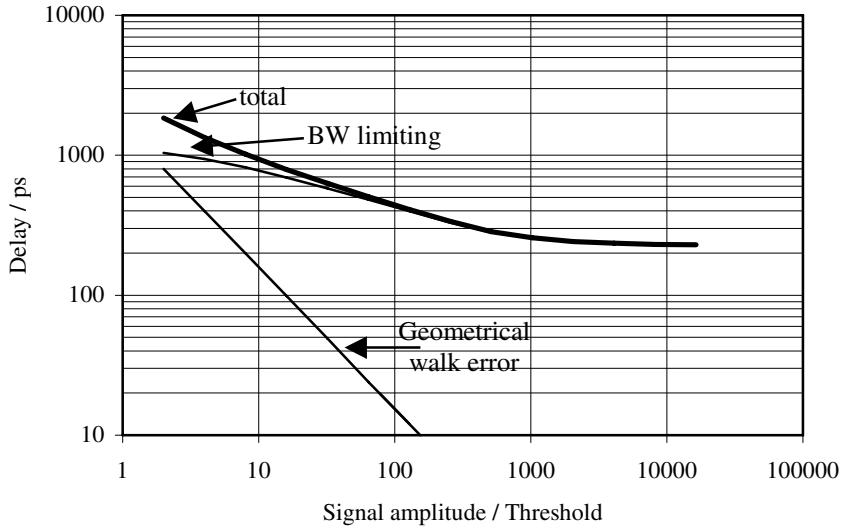


**Fig. 5. Delay in the timing point of the leading edge discriminator as a function of signal level.**

The walk error is 1.6 ns when the amplitude of the input signal varies from 2 times to 10 000 times the threshold level (1:5000) and saturates at that level. The error in the range from 2 to 40 which is the linear range of the receiver channel, can be compensated for by means of correction table obtained by measuring the amplitude of the pulse. This compensation would reduce the walk error by 1.2 ns, so that the uncompensatable walk error is 400 ps, corresponding to a distance of 60 mm (±30 mm). The residual walk error

is small enough for some applications, but a more accurate timing discriminator has to be used in short range applications in particular. The benefits of the leading edge discrimination method are its simplicity, the wide dynamic range of the input signal and the possibility to perform the measurement with a single pulse without any gain adjustments or information about the level of the incoming pulse. The walk error can be reduced by increasing the bandwidth of the receiver and shortening the rise time of the optical pulse.

Another important parameter for timing discriminators is jitter, which defines the statistical error in the timing point. The timing jitter $\sigma_t$, representing the standard deviation of the distribution of the measurements, can be calculated using the triangle rule (Bertolini 1968)

$$\sigma_t = \frac{\sigma_v}{\left.\frac{d}{dt} v(t)\right|_{t=t_p}}, \tag{3}$$

where $\sigma_v$ is the noise power at the timing point $t_p$ and $v(t)$ is the input signal of the timing comparator. The noise in the equation usually originates from the noise of the receiver channel electronics. The jitter is largest with the smallest input signals, but is still smaller than the walk error in the leading edge detection method. A rise time of 1.6 ns, for example, and a peak signal amplitude to rms-noise level ratio (SNR) of 10, which represents the smallest usable signal level, will results in a precision of about 160 ps (24 mm, σ-value). This can be improved by averaging single measurements, which results in an improvement of $\sqrt{N}$, where N is the number of averaged asynchronous measurements (Hewlett-Packard AN 162-1).

## 2.2 High-pass timing discrimination

In high-pass timing discrimination the timing point is generated from a unipolar input pulse using a high-pass filter, as shown in Fig. 6a. The zero-crossing point of the bipolar output signal defines the timing point, which is insensitive to variation in the amplitude of the input signal as long as the signal is processed in a strictly linear manner, i.e. the pulse is not distorted in the receiver. Thus the discrimination will not have the same walk error as leading edge discrimination. When the amplitude of the signal varies, the slew rate and over/underdrive around the timing point will change. As the propagation delay of a comparator depends on these parameters, the timing comparator will generate walk error basically for the same reasons as explained above (Binkley & Casey 1988). The walk error is nevertheless much smaller than that of a leading edge discriminator and its level depends on the speed of the comparator and decreases with the scaling of process technologies.

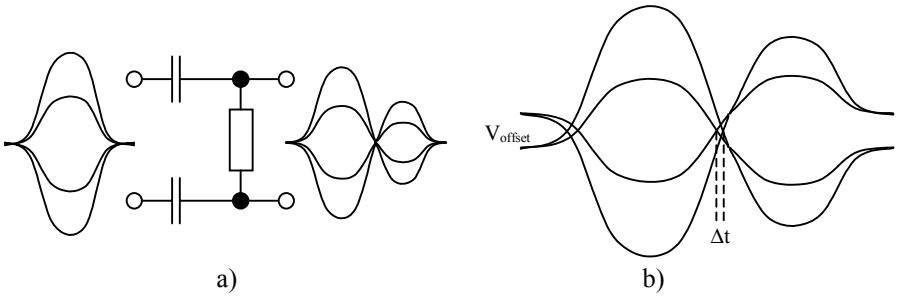


**Fig. 6. a) Schematic diagram of a high-pass filter and its input and output signals, and b) change in the timing point with offset voltage.**

The walk error can be partly compensated for with an offset voltage arranged at the input to the timing comparator, so that a signal with a small amplitude will have its zero-crossing point slightly earlier than signals with larger amplitudes, as shown in Fig. 6b (Kinbara & Kumahara 1969). The compensation is not ideal, but it does reduce the walk error significantly in the useful region, as shown in Fig. 7.

The effect of walk error compensation is shown in Fig. 8, where the walk error is measured for an integrated receiver channel with four offset voltages (Paper VIII). The increase in the error at larger signal amplitudes is caused by distortion of the pulse in the amplifier channel.

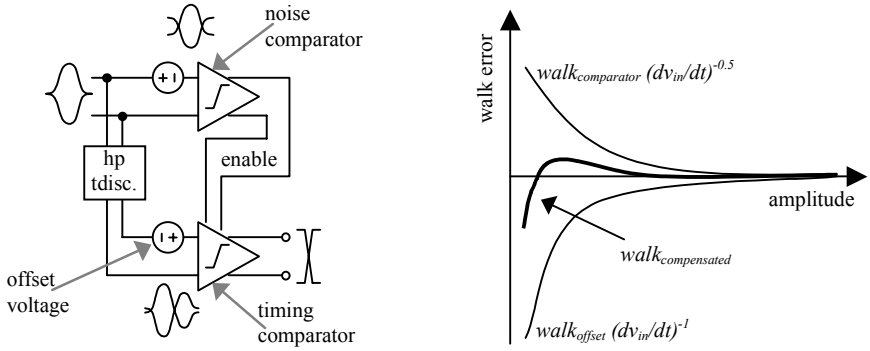


**Fig. 7. Coarse schematic diagram of a high-pass timing discriminator with offset voltage.**

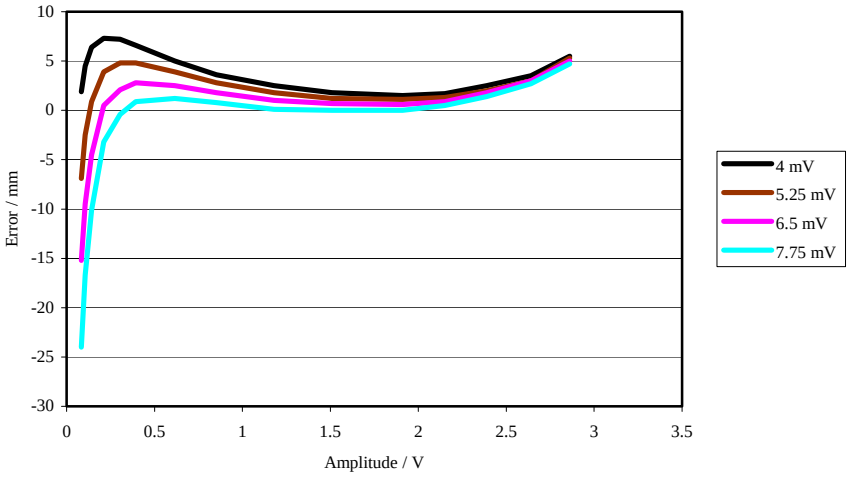


**Fig. 8. Measured walk error of a high-pass timing discriminator as a function of offset voltage.**

A noise comparator is needed in the high-pass timing discriminator to prevent noise from causing false triggerings, whereas the leading edge discriminator requires no noise comparator at all. In practise the minimum usable SNR is about 10 for a high-pass timing discriminator (Ziemer & Tranter 1985) and should be slightly more for a leading edge discriminator so that the walk error and jitter should not be too high. On the other hand, the maximum signal level in high-pass timing discrimination is limited by the linear dynamic range of the receiver and usually has to be extended with gain control structures.

The jitter in high-pass discrimination depends on the shape of the pulse and on the bandpass corner frequencies of the receiver. Simulations indicate that a high-pass corner frequency of about 30% of the receiver channel bandwidth will give a good compromise between small walk error and small jitter and the level of the jitter is comparable to that in leading edge discrimination.

As the walk error is an important topic in the design of laser radar receivers, a new idea for combining timing discrimination (high-pass timing discriminator) and time interval measurement was developed to avoid the problem, as presented in section 3.1.3.

# 3 The laser radar module

This chapter describes the progress of the work in terms of the original papers included at the end of the thesis. Receiver channels with different timing discriminators implemented in full-custom ASICs are presented in section 3.1. The functionality and usability of the circuits could then be verified by constructing laser rangefinder prototypes which utilised the receiver ASIC. The prototypes are described in section 3.2.

Since a small laser radar module would also need integration of its photodetector and time interval measurement systems, integration of a high-speed photodetector into a standard CMOS/BiCMOS process was investigated, as presented in section 3.3. Finally a single chip realisation of the receiver and time interval measurement functions of a pulsed time-of-flight laser radar is described in section 3.4. The chip can measure distance not only from one target but in three directions simultaneously.

## 3.1 Receiver channel electronics

Three methods of timing discrimination were verified by designing and testing integrated circuits. These circuits included a receiver employing high-pass timing discrimination, a receiver employing a leading edge discriminator and a receiver in which timing discrimination and time interval measurement were combined. The circuits are described in the following sections, together with some measurement results.

### *3.1.1 Receiver with a high-pass discriminator*

The structure of the receiver channel design described in paper I is shown together with a photograph of the circuit in Fig. 9. The receiver consists of two identical channels, one for the start pulse and the other for the stop pulse, integrated on the same chip so as to minimise errors caused by delay variations due to changes in temperature, supply voltage

or process parameters. An external avalanche photodiode (APD) is used to convert the optical pulse to a current pulse. The noise level at the output to the preamplifier is 1 mV and the maximum linear amplitude is about 1.5 V. Thus the transimpedance preamplifier limits the dynamic range of its input signal to about 1:150 (SNR>10). A current mode gain control cell (CMGC) has been used successfully between the photodetector and the preamplifier to enlarge the dynamic range of the input signal up to 1:620. The cell acts as a current buffer with variable attenuation, and the change in attenuation causes only a little variation in the propagation delay and bandwidth (Gilbert 1968, Vanisri & Toumazou 1995, Ruotsalainen *et al.* 1999b). This property is very important in time-of-flight rangefinding, as any change will directly affect the distance result, with 6.7 ps corresponding to 1 mm. After the CMGC cell, the current pulse is converted to a voltage pulse in a low-noise transimpedance preamplifier and then amplified in two double-stage voltage amplifiers (Cherry & Hooper 1963) which have offset compensation circuitry with three selectable offset voltages. A further reduction in the dynamics of the signal is achieved with a voltage mode gain control cell (VMGC, R-2R ladder) between the preamplifier and the voltage amplifier. Finally, the high-pass timing discriminator generates a logic-level timing pulse for the TDC. The chip was implemented in an AMS 0.8 μm BiCMOS process.

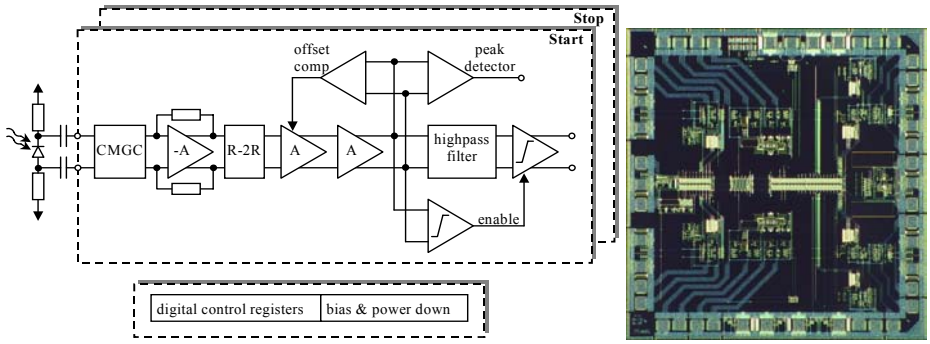


**Fig. 9. Diagram and photograph of the receiver circuit, comprising the start and stop channels.**

The operation of the gain control is shown in Fig. 10, in which the x-axis shows the current pulse amplitude at the input to the receiver and the y-axis the voltage pulse amplitude at the input to the timing discriminator.

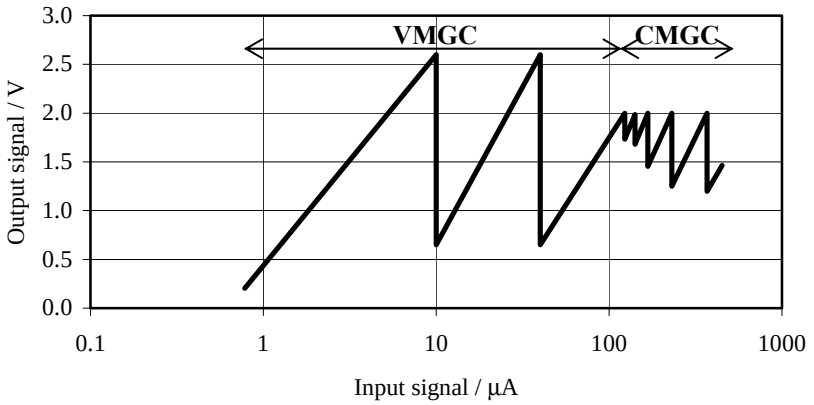


**Fig. 10. Output signal from the amplifier channel as a function of the input signal when gain controls are used.**

The signal is first attenuated with voltage mode gain control in order to keep the SNR as large as possible, and current mode gain control is used when the transimpedance preamplifier begins to saturate. The figure shows that the 1:600 dynamic range of the input signal has been reduced to 1:13, which is acceptable for the timing discriminator. Measurements performed using the circuit as a part of a laser radar device are summarised in Table 1.

*Table 1. Performance of the receiver channel with a high-pass timing discriminator.*

| | |
|---|---|
| Bandwidth | 170 MHz |
| Maximum transimpedance | 260 kΩ |
| Input referred noise | 6 pA/√Hz |
| Delay variation with current mode gain control | ±5 ps ($A_i$ = 1–1/15) |
| Delay variation with voltage mode gain control | ±10 ps ($A_u$ = 1/4–1/16) |
| Walk error of the timing discriminator | ±12 ps ($u_{in}$ = 0.25V–2.6V) |
| Total drift with temperature | 3 ps (average in the range –5°C – +40°C) |
| Single-shot precision, 2 channels, σ-value | 240 ps ($SNR_{start}$ = 125, $SNR_{stop}$ = 20) |
| | 58 ps ($SNR_{start}$ = 125, $SNR_{stop}$ = 250) |
| Chip size | 3mm x 3mm |
| Power consumption (without power down) | ~ 280 mW |

The total accuracy, taking into account the walk error (signal varies in a range 1:620) and jitter, is about ±4.7 mm (average of 10 000 measurements), and the temperature drift is less than ±3 ps (±0.5 mm) in the temperature range from –5°C to +40°C. The accuracy can be further improved by compensating for the dominant error sources, i.e. the walk error and voltage mode gain control error, by using a correction table together with

information on the amplitude of the signal, measured with the peak detector included in the chip. The current consumption is ~ 50 mA from a 5 V supply and ~ 3 mA from a –10 V supply.

Electronic gain control structures can be used to replace optical ones in some applications, which along with the small size and low power consumption achieved by the use of integrated electronics, simplifies the construction of the resulting rangefinding devices.

### *3.1.2 Receiver with a leading edge discriminator*

The structure of the single channel receiver described in paper II is shown in Fig. 11. The circuit is implemented in an AMS 0.8 µm BiCMOS process and is intended for an industrial application in which the dynamic range of the input signal is large (as high as 1:4000) and the measurement has to be made with a single optical pulse without any prior information about the signal amplitude. This means that gain control structures are useless. The circuit employs a leading edge discriminator with a constant threshold voltage. The amplitude of the received pulse is measured with a peak detector and the information is used to compensate for the walk error. Fully differential structures were used in the receiver channel and in the timing discriminator in order to reduce sensitivity to disturbances, improve common mode rejection, power supply rejection and linearity, reduce inductance of the input bond wires due to mutual inductance etc.

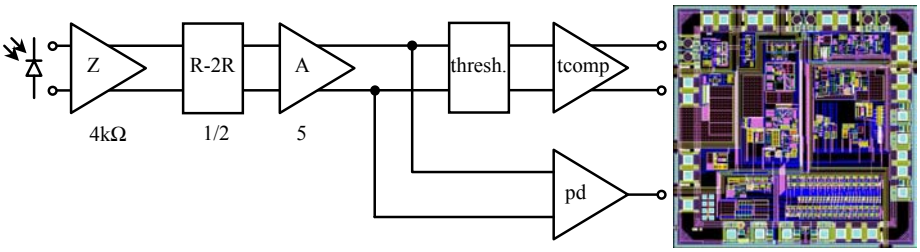


**Fig. 11. Diagram and photograph of the receiver with a leading edge discriminator.**

The measurements were performed using the circuit as a part of a laser radar device, which achieved centimetre-level single-shot accuracy over a wide dynamic range. The accuracy of a single measurement is better than ±45 mm, including walk error (amplitude of the input signal varies in the range 1:4000), drift with temperature (ambient temperature varies in the range 0°C to +50°C) and jitter (σ-value, SNR > 35). Due to the wider bandwidth, 250 MHz, the jitter is smaller than that of receiver channel using a high-pass timing discriminator described in section 3.1.1, but the walk error is larger because of the different timing discrimination method.

The walk error measured at three temperatures, after compensation, is shown in Fig. 12. The origin of the walk error was not completely understood at the time of writing paper II, but it can be easily explained in terms of the theory presented in section 2.1, as

the uncompensatable walk error, ±30 mm, agrees well with the walk error simulated in that section. The parameters used in the simulation are equal to those of the receiver channel and to the properties of the optical pulse used in the measurements.

The circuit contains real-time calibration and testing structures to ensure the correctness of the distance result. The circuit is well suited for applications in which distance has to be measured with a single pulse, the amplitude of which cannot be predicted from previous measurements. The measurement results are summarised in Table 2.

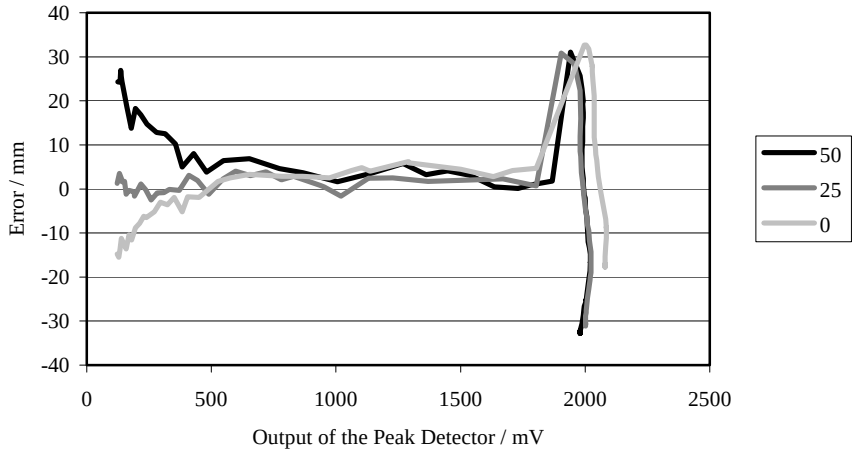


**Fig. 12. Error in distance measurement after temperature and walk error compensation at different temperatures.**

*Table 2. Performance of the receiver channel with a leading edge discriminator.*

| | |
|---|---|
| Bandwidth | 250 MHz |
| Transimpedance | 10 kΩ, 20 kΩ, 40 kΩ, selectable |
| Input referred noise | 7 pA/√Hz |
| Walk error after temperature and walk error compensation | ±35 mm ($i_{in}$ = 1:4000) |
| Single-shot precision, σ-value | < 9.5 mm (*SNR* > 35) |
| Chip size | 2.5 mm x 2.4 mm |
| Power consumption | ~ 270 mW |

A photodiode with a large area (diameter ~500 μm) is usually needed in industrial measurement applications, and this brings a capacitance of about 2 picofarads into the input to the preamplifier. In addition, the interconnection between the photodetector and the receiver includes structures such as ESD protection, an I/O pad and PCB wiring, which entail an additional capacitance of several picofarads. The large capacitance

generates a voltage noise peaking in the preamplifier and calls for a careful design in order to ensure stability with a large bandwidth.

### *3.1.3 Combining a timing discriminator with TAC*

As the comparator proved to be the source of the walk error, a new topology was developed in which timing discrimination and time interval measurement are combined and no comparator is used at all (Paper III). The timing point of the pulse is produced using a C-R high-pass filter and is free of walk error. A fast comparator is usually then used to detect the timing point and to produce a logic-level signal for the TDC, which can be a time-to-amplitude converter (TAC) followed by an A/D converter, for example, or a TDC based on digital delay cell topologies.

In the new method presented in paper III time interval measurement is based directly on linear signal processing of the timing pulses of the receiver channel. The idea is to steer the input transistors of the TAC directly with the variable slope analogue signal which is usually connected to the comparator. Thus the input transistors of the TAC are used as "analogue switches" instead of merely as current switches. It will be shown in the following paragraphs that even if the amplitude of the input signal varies, the time-to-amplitude conversion will give the same result, i.e. the method is free of walk error.

A coarse schematic diagram of a differential pair which serves as the core element of the TAC is shown in Fig. 13. Time to amplitude conversion is produced by discharging a capacitor *C1* with a current $I_b$ for as long as the input signal $V_{in}$ is positive. Before each measurement the level of $V_{out}$ is reset to a positive supply with a switch *S1*. The change in the amplitude $\Delta V_{out}$, which corresponds to the time interval, is measured with an A/D converter.

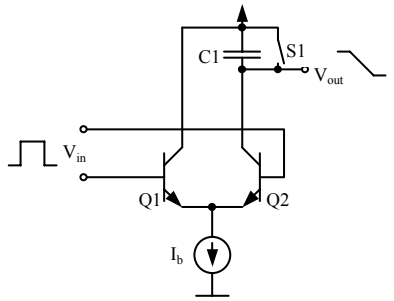


**Fig. 13. Schematic diagram of the differential pair.**

The immunity to walk error is presented in Fig. 14 with the aid of a large signal transfer function for the differential pair. The input signals to the TAC $V_{in}$ are shown as a function of time in the bottom left panel of Fig. 14. The start edge of the time interval to be measured is constant, whereas the slew rate of the stop edge varies as a function of the amplitude of the received signal. The input voltage signals are converted to the output

current signals $I_{out}$ shown in the top right panel of the figure using the large signal transfer function of the differential pair shown in the top left. Finally the output currents are integrated as a function of time, shown in the bottom right corner. The integral corresponds to the voltage drop at the output, $\Delta V_{out}$. As can be seen in the figure, the result of the integration is independent of the slew rate at the stop edge, which means that the distance result does not depend on the amplitude of the received signal (which causes variation in the slew rate of the falling edge) and therefore has no walk error.

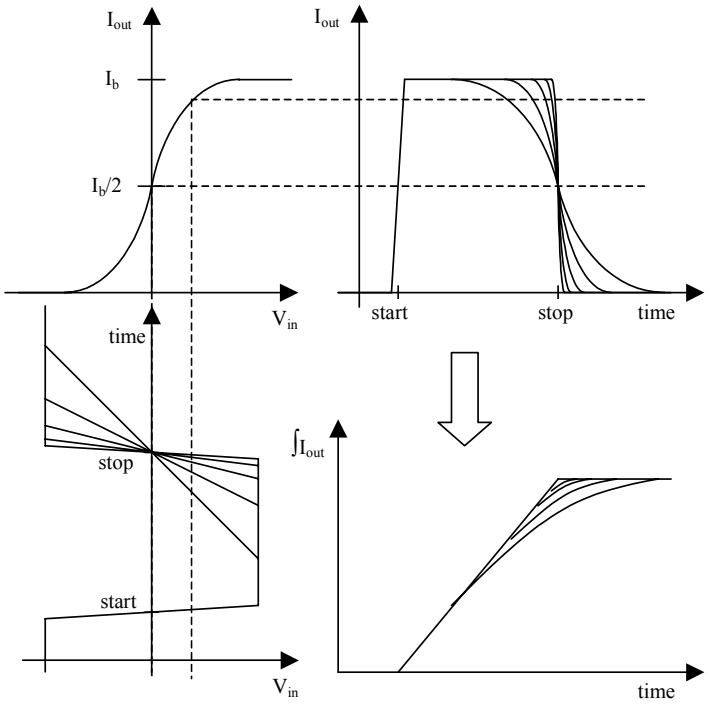


**Fig. 14. Operation of the TAC with different slew rates of the stop signal.**

In order to be able to make use of the proposed method, the receiver channel should produce the pulse presented in the bottom left panel of Fig. 14 from the original unipolar timing pulse. This is achieved by the receiver channel construction shown in Fig. 15. For simplicity, the receiver and signals are drawn in a single-ended form, whereas the implementation of the test chip was differential.

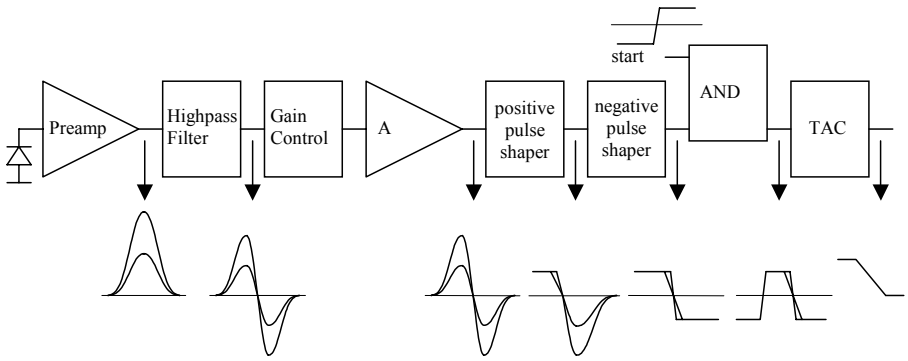


**Fig. 15. Building blocks and signals of the receiver channel.**

A bipolar pulse is generated from the unipolar input pulse using a similar high-pass filter to that described earlier in section 2.2. In order to achieve a large gain-bandwidth product and to process the pulses and the ramp signal linearly, the signal swing in the blocks is limited to ±400 mV and the gain of the amplifying stages is set to about 2 with emitter degeneration resistors. To pick up the rampsignal around the zero-crossing point of the bipolar signal, structures have to be used which will force the signal to be positive before the pulse and negative after the pulse (the positive and negative pulse shaper blocks in Fig. 15). This can be done using the circuitry shown in Fig. 16. The upper part of the diagram shows a limiter block with a force function and the lower part the latch circuitry which detects the edge of the bipolar pulse and controls the force function. The level of input signal which changes the state of the latch can be set with the adjustable bias current source.

The receiver (and also the latch) must be reset before measurement, whereupon the latch forces the output of the circuitry to be positive (+400 mV). When the input signal exceeds the preset offset voltage of the latch, the state of the latch changes and the output of the circuitry begins to follow the bipolar input signal. In the same way, but in opposite order, the negative part of the bipolar pulse is formed with similar circuitry (negative pulse shaper). The output of the circuitry first follows the input signal, and when the negative part of the bipolar signal crosses the negative offset voltage of the latch, the output is forced to be negative (–400 mV). Finally the start signal is included and the signal shown in the bottom left panel in Fig. 14 is produced for the time to amplitude converter.

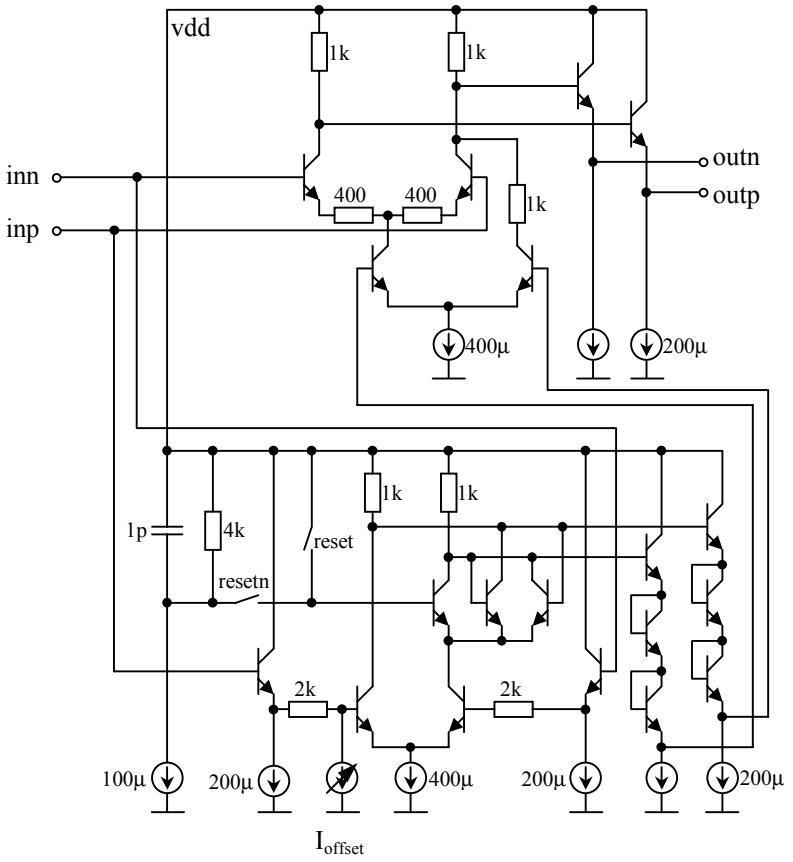


**Fig. 16. Diagram of the circuitry used to distinguish the ramp signal.**

The voltage drop at the output to the TAC is measured with an A/D converter. If a resolution of one millimetre (~7 ps) is needed and a 12-bit A/D converter is being used, the maximum integration time will be about 27 ns. This will result in a measurement range of about 4 metres. The range can be increased without detracting from the resolution by using a coarse counter to count the periods of a reference clock and interpolating the timing point inside the clock period using the scheme presented. Two TACs are needed for this kind of structure, the rising edges of their input signals being produced by the start and stop pulses and the falling edges by the reference clock.

The operability of the idea was verified by implementing a test circuit in a 0.8 µm BiCMOS process (paper III). The measured walk error is shown in Fig. 17 and the time result varies ±3.5 ps (±0.5 mm in distance) with an input signal dynamic range of 1:21. The error is smaller than the ±12 ps walk error of the high-pass timing discriminator in a dynamic range of 1:10. The dynamic range of this new method is limited by the finite bandwidth and slew rate of the receiver channel. The duration of the "ramp signal" changes from about 2 ns to 100 ps.

The single-shot precisions of the conventional channel and the new channel are of the same magnitude, but the scheme involves no very fast, power consuming switching operations, which means that the circuitry produces less disturbances. The idea enables walk error to be reduced, especially at small signal amplitudes and allows the level of integration of the system to be increased still further.

The new scheme was not used in the laser rangefinder prototype devices whose construction is described in the following section, because a new test circuit should have been designed to enlarge the measurement range by means of a reference clock and interpolation inside the clock period. As the receiver channel with a high-pass discriminator and a separate TDC chip were already available, these were used in the prototypes.

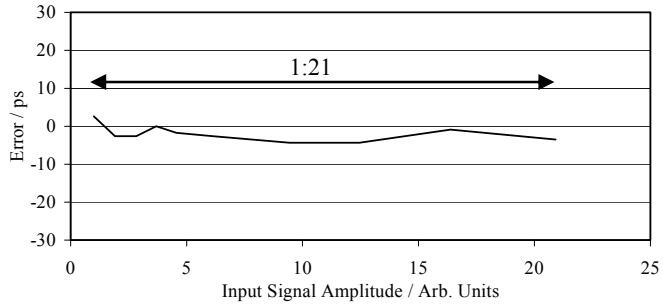


**Fig. 17. Measured walk error of the receiver channel.**

## 3.2 Laser rangefinding device

In order to verify the utility of the integrated receiver chips, three prototypes of portable pulsed TOF laser rangefinding devices were constructed. Their smaller size and power consumption relative to the laser rangefinding device constructed using discrete components in electrical parts, shown in Fig. 1a, would also open up new possible applications. The prototypes are presented in papers IV, V and VI (the device described in paper VI is shown in Fig. 1b). The first prototype, presented in paper IV, employs PIN diodes as photodetectors and has the optics integrated into the device, whereas the prototypes presented in papers V and VI make use of APDs and a separate optomechanical measurement head. Typical of all the prototypes was the aim to reduce power consumption, weight and size by means of application-specific integrated circuits (ASICs).

In the first prototype a bare laser diode was used without mixing the signal with optical fibres. This reduces the accuracy, because of the inhomogeneity of the laser beam, but is very simple and easy to construct and is accurate enough for the cm-level accuracy

aimed at in that device. In the other prototypes, where the optomechanical measurement head is used, the connecting fibres homogenise the laser beam (Määttä *et al*. 1990). The length of the fibres, 2 metres, is enough to mix the modes of the beam and the separate measurement head makes it possible to design it with consideration for the requirements of the application (Määttä *et al*. 1990). The measurement process is controlled using a microcontroller (Motorola MC68HC11) in the first prototype and a FPGA circuit (Altera EPM 7032LC44-6) in the other two devices. A block diagram of the device presented in paper VI is shown in Fig. 18.

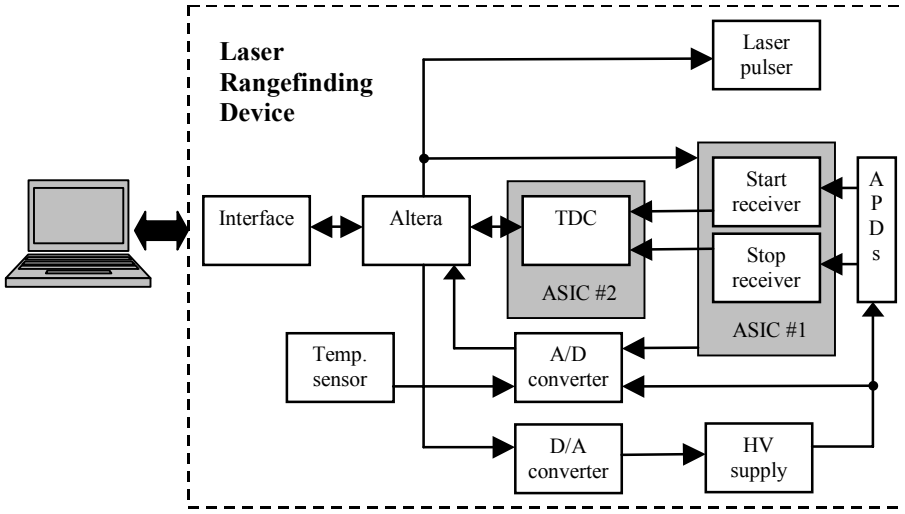


**Fig. 18. Block diagram of laser rangefinder described in paper VI.**

The laser pulse transmitter produces an optical pulse after triggering. The trigger signal in the laser radar device developed in paper VI is optical, in order to reduce the interference between the laser pulse transmitter and the other electronics which was recognised with previous prototypes using electrical triggering. The diode used in the transmitter is a multi-quantum well InGaAs pulsed laser diode (PerkinElmer PGAS3S06), which needs a short current pulse of a few tens of amperes in order to give a short, powerful optical pulse. The current pulse is generated by charging a capacitor to 300V with a transformer and then switching the laser diode and the capacitor in series with an avalanche transistor (Zetex FMMT415). The electronics of the laser pulse transmitter additionally generate time jitter in the switching event, thus preventing it from being synchronous with the clock of the TDC, as asynchronous measurement is essential in order to be able to improve the measurement result by averaging (Hewlett-Packard AN 162-1).

The laser diode is coupled to a transmitter fibre (diameter 365 μm) with a pair of lenses and the peak power of the optical signal is 110 W, the FWHM 6.7 ns and the rise and fall times 2.7 ns and 3.0 ns at the output of the fibre. The wavelength of the optical pulse is 905 nm and the pulsing frequency 10 kHz, which gives an average power of 7.4 mW. The optical pulse, measured using a sampling oscilloscope with an analogue bandwidth of 15 GHz, is shown in Fig. 19.

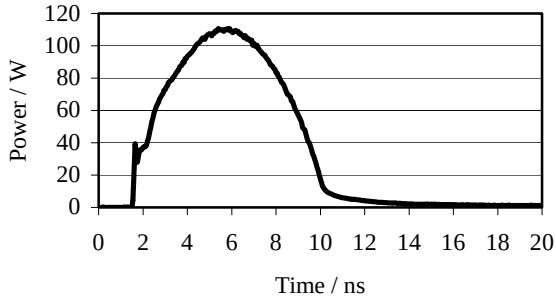


**Fig. 19. Optical pulse of the laser pulse transmitter described in paper VI.**

The devices described in papers V and VI employ the receiver channel described in paper I. The linearity error of the device described in paper VI was measured using a calibration track with an accuracy of 1 mm. The measured error together with the amplitude of the stop signal at the input to the timing discriminator are shown as a function of distance in Fig. 20.

The non-linearity at distances shorter than ~10 metres is caused by the vignetting phenomenon of the dual-axis optics used in the measurements (Määttä *et al*. 1990). At short distances the receiver sees only a small portion of the light spot on the target, actually the portion that comes from the edge of the spot, and these modes of light have travelled a longer way in the fibre, which means that the target seems to be further away. At distances shorter than 3.8m the signal was too weak for measurement with the optics used here. The optics can be customised for the application, and thus the measurement range can also be modified.

The ripple in the amplitude of the signal is caused by the electrical current-mode gain control, which tries to keep the signal at a level of 1.5 V (paper VI). The dynamic range of the optical input signal in the linearity measurement was 1:11 (@ 3.8…33.8 m).

The single-shot precision was calculated from a large number of single-shot measurements at a fixed distance. The level of the input signal, and thus the peak signal amplitude to rms-noise level ratio (*SNR*), was varied using an optical neutral density filter. The standard deviation of the distance results as a function of *SNR* is shown in Fig. 21.

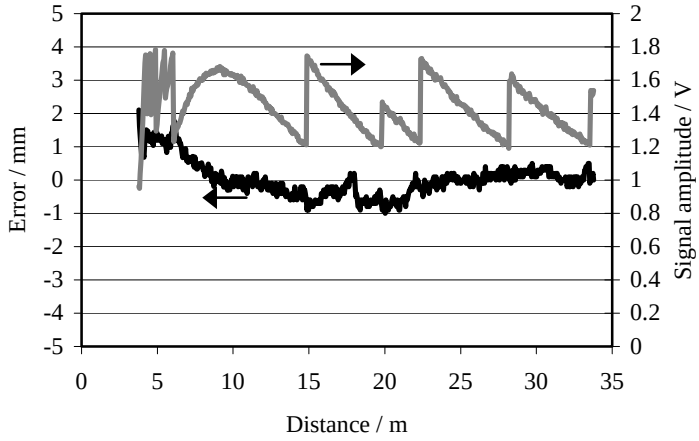


**Fig. 20. Linearity error and amplitude of the stop signal of the rangefinding device described in paper VI.**

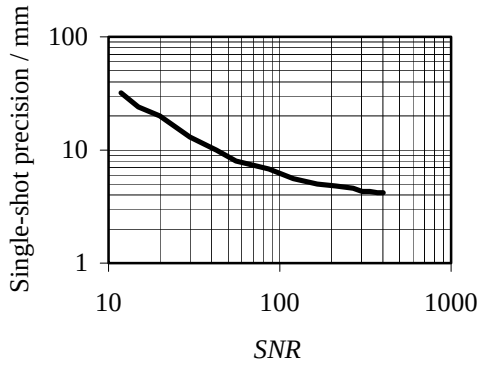


**Fig. 21. Single-shot precision of the rangefinding device described in paper VI.**

The curve in the figure saturates to a level of 4.2 mm with large signals, which is the single-shot precision of the TDC used in the device. The performance of the laser rangefinding devices is summarised in Table 3.

*Table 3. Performance of the laser rangefinding devices.*

| | Paper IV | Paper VI |
|---|---|---|
| single-shot precision, σ-value | < 140 mm | 40 mm (SNR = 10)<br>6 mm (SNR = 100) |
| linearity error | < 40 mm (1 … 30 m) | ±1.5 mm (3.8 … 33.8 m) |
| temperature drift p-p | 22 mm (−10 … +50°C) | 4 mm (−10 … +50°C) |
| power consumption | 0.84 W | 3.5 W |
| measurement frequency | 2.1 kHz | 10 kHz |
| Current-mode input signal range | 1.5 ... 110 μA (1:70) | 0.64 ... 410 μA (1:640) |
| Analogue bandwidth | 100 MHz | 130 MHz |
| Analogue transresistance | 7.3 ... 100 kΩ | 0.91 ... 263kΩ |
| Input referred noise | 15 pA/√Hz | 5.6 pA/√Hz |

The TDC, which converts the time interval between the logic-level start and stop signals to a digital word, was implemented in an AMS 0.8 μm BiCMOS process, the size of the chip being 12 $mm^2$. It operates by digitising the time interval roughly using an 8-bit counter clocked by a 100 MHz external oscillator. This allows a large measurement range. The resolution is improved by interpolating the timing event inside the clock period by means of a dual ramp technique (Räisänen-Ruotsalainen *et al.* 2000), the final single-shot precision being less than 30 ps, which corresponds to a distance of 4.5 mm. The measured non-linearity of the TDC is ±5 ps in a measurement range from 10 ns to 2.5 μs, which corresponds to less than ±1 mm in the range from 1.5 m to 370 m. The temperature drift is smaller than ±6 mm (±40 ps) in the temperature range –40 to +60°C. The current consumption of the TDC without the external 100 MHz oscillator is 70 mA from a single 5 V supply (350 mW), and its maximum measurement frequency is 150 kHz.

The amplifier channel and the TDC used in the prototype presented in paper IV are described in more detail by Ruotsalainen *et al.* (1995) and Räisänen-Ruotsalainen *et al.* (1995) and the receiver channel and the TDC of that in paper VI by Palojärvi *et al.* (1997) and Räisänen-Ruotsalainen *et al.* (2000).

There are not many papers on pulsed TOF laser rangefinding devices in the literature. Samuels *et al.* (1992) reported on a low-cost, hand-held laser rangefinder for speed detection and law enforcement. The accuracy required in its absolute distance measurements was not very high, as the target would be moving and the primary object of interest was the speed. The resolution of the device was 2.5 feet (~75 cm). The authors decided to use the pulsed TOF topology because a construction using CW techniques with the needed specifications would not have been an eye-safe Class 1 laser product. The parameters of the laser pulser, 30 W output pulse power, a pulse width of 20 ns and a repetition rate of 381 Hz, gave an average output power of 0.23 mW.

Araki & Yoshida (1996) reported on a pulsed time-of-flight optical distance meter for measuring molten steel levels. The measurements were also performed using a piece of black paper as a target, and the measurement range and standard deviation of the measurement error were 1 m and 1 mm respectively.

A commercial pulsed time-of-flight distance meter is available from Banner Engineering Inc. A visible red laser diode is used to produce a pulse with a duration of 10 ns, and the measurement range is from 0.3 m to 5 m with diffuse targets with ±30 mm linearity. The device is intended especially for industrial automation applications.

## 3.3 Integration of the photodetector

Integration of the photodetector into the same chip with the rest of the electronics entails several advantages. The stability of the receiver is improved, because the large parasitic capacitance and inductance between the photodetector and the input to the transimpedance preamplifier are reduced drastically. In addition, the bandwidth can be increased and the noise, size and mechanical complexity reduced. Production costs would also be lower, because the number of components decreases if the photodetector can be integrated into the same process without any process modifications.

The wavelength of the powerful semiconductor laser diodes used in pulsed TOF laser rangefinders (GaAs or AlGaAs) is 850...900 nm, so the optical signal can be detected using a silicon photodiode and will not limit implementation on the same chip as the rest of the receiver circuit. The size of the laser diode is ~100µm...300µm, and that of the photodetector should be of the same order if the optical parameters on the transmitter and receiver sides are equal.

The photodetector should be as sensitive as possible. An avalanche photodiode would give a higher response than conventional pin photodetectors because of internal gain. Integration of an APD is possible in standard processes and it gives a gain factor of up to thousand, but at the same time the excess noise factor rises to a level which prevents its use for pulsed TOF laser radar (Biber *et al*. 2001).

Several papers have been published in which photodiodes for wavelengths of 750–850nm have been integrated into silicon processes. These, together with the most important parameters, are summarised in Table 4.

*Table 4. Comparison of Silicon Integrated Photodiodes at NIR wavelengths.*

| R<br>A/W | η | λ<br>nm | Process<br>µm | BW /<br>$t_r/t_f$ | $V_{PD}$<br>V | Ref. |
|---|---|---|---|---|---|---|
| 0.54[1] | 0.82[1] | 850 | Mod.<br>1.0 NMOS | 150 MHz | 32 | Schow *et al*. 1999 |
| 0.35 | 0.56 | 780 | Mod. CMOS | 7.24/11.8 ns | 3 | Zimmermann 1996 |
| 0.40 | 0.64 | 780 | Mod. CMOS | 1.26/1.27 ns | 3 | Zimmermann 1996 |
| 0.42 | 0.67 | 780 | Mod. CMOS | 0.63/0.7 ns | 3 | Zimmermann 1996 |
| 0.35 | 0.56 | 780 | Mod. Bipolar | 300 MHz | 3 | Yamamoto *et al*.<br>1995 |
| 0.5[1] | 0.78[1] | 800 | Mod. Bipolar | 680 MHz | 10 | Kyomasu 1995 |
| 0.40 | 0.64 | 780 | Mod. BiCMOS | 0.26/0.22 ns | 20 | Zimmermann 1996 |
| 0.09 | 0.13 | 840 | SOI Bipolar | 1200 MHz | 5 | Ghioni *et al*. 1996 |
| 0.29 | 0.46 | 780 | 1.0 CMOS | 3.83/6.18 ns | 3 | Zimmermann 1996 |
| 0.04 | 0.06 | 850 | 0.35 CMOS | 1 Gb/s | 10 | Woodward *et al*.<br>1998 |
| **0.28** | **0.41** | **850** | **0.8 CMOS** | **< 5 ns** | **3.5** | **Paper VII** |
| 0.045 | 0.07 | 850 | 0.8 Bipolar | 3 Gb/s | | Wieland *et al*. 1994 |
| 0.07 | 0.10 | 850 | 0.6 BiCMOS | 700 MHz | 2.5 | Lim *et al*. 1993 |
| **0.31** | **0.45** | **850** | **1.2 BiCMOS** | **30ns** | **5.0** | **Paper VII** |

1) Anti-reflection coating

The first eight lines of the table represents realisations in modified processes, whereas the last six lines show realisations without process modifications. Schow *et al*. (1999) reported on a lateral, interdigitated p-i-n photodiode fabricated directly on a high-resistivity n-type substrate. Zimmermann (1996) reported on several different photodiodes. That implemented in an unmodified 1.0µm CMOS twin-well process is a vertical $n^+/p^-/p^+$ substrate photodiode. The three modified photodiodes are based on the same process but with changes in the thickness and concentration of the $p^-$ epitaxial layer. The best result has been achieved using a vertical $p^+/n^-/n^+$ substrate photodiode in a modified 1.0µm CMOS twin-well process. Yamamoto *et al*. (1995) reported a vertical $p^+/n^-/n^-/n^+$-buried p-i-n photodiode in modified bipolar technology. The two $n^-$ layers are grown by high-resistive epitaxial layer formation. Kyomasu (1995) reported a vertical $n^+/p^-/p^+$ photodiode in modified bipolar technology, where $p^-$ and $n^+$ are epitaxial layers and the thickness of the high-resistivity $p^-$ layer is 30µm. Ghioni *et al*. (1996) reported on a lateral, interdigitated p-i-n photodiode on SOI, which is not usable in a standard manufacturing process.

Woodward *et al*. (1998) reported a $p^+$/n-well photodiode implemented in a standard process in which interdigitated $p^-$ diffusion fingers inside the n-well form the active terminal. This enabled a higher speed to be obtained at the expense of responsivity, as the slow diffusion current tail originating from carriers diffusing from the $p^-$ substrate was screened away. Wieland *et al*. (1994) reported a photodiode using base and collector layers in bipolar technology. The detector was surrounded by a $p^+$ substrate ring to help to

collect the carriers generated below the base-collector junction and to keep crosstalk low, but this also reduced the quantum efficiency. Lim *et al*. (1993) reported a vertical $p^+$/n-well/$n^+$-buried layer p-i-n photodiode in which the thin (0.7 μm) "intrinsic" region could be depleted with a low bias voltage.

The photodiode implemented in 0.8μm CMOS technology presented in paper VII employs $n^+$/n-well/$p^-$/$p^+$ substrate layers. The $p^-$ layer is epitaxially grown and is part of a standard n-well CMOS process. A cross-section of the photodiode is shown in Fig. 22.

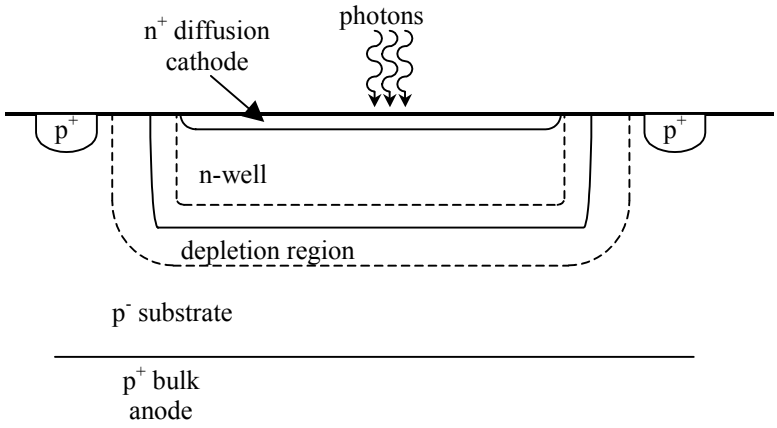


**Fig. 22. Cross-section of the pn-photodiode integrated in a 0.8 μm CMOS process.**

The measured rise time of the photodiode was ~ 5 ns and the responsivity ~ 0.3 A/W. As the rise time of the preamplifier itself was about 4 ns, that of the photodiode must have been even less than 5 ns (paper VII).

A cross-section of the photodiode implemented in 1.2μm BiCMOS technology presented in paper VII, which uses $n^+$/n-well/$n^+$buried/$p^-$ substrate layers, is shown in Fig. 23.

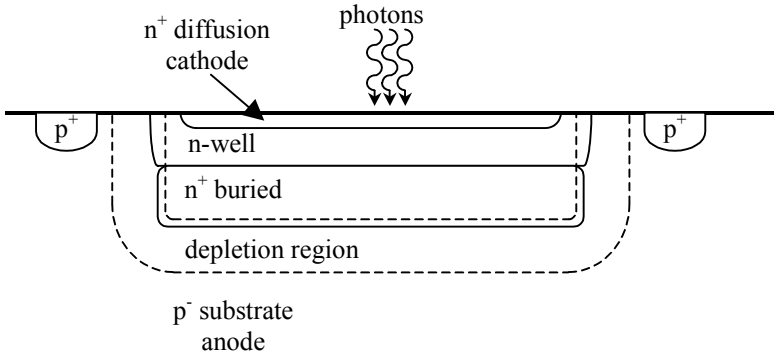


**Fig. 23. Cross-section of the pn-photodiode integrated in a 1.2 μm BiCMOS process.**

The measured rise time of the photodiode was ~ 30 ns and the responsivity ~ 0.3 A/W. A pulse response consists of two parts: the fast rising edge of the output pulse caused by the drift current and a slow part caused by diffusion currents. Thus the effective responsivity is reduced in our application, where the length of the optical pulse (fwhm < 10 ns) is shorter than the rise time. The slow current tail in the response does not matter when the pulsing frequency is low compared with the lifetime of the minority carriers, i.e. all the minority carriers recombine before the next optical pulse arrives.

The main difference between the two processes described in paper VII from the point of view of the photodetectors is that the CMOS process has a highly doped $p^+$ bulk below the epitaxially grown, lightly doped $p^-$ substrate while the $p^-$ substrate in the BiCMOS process is lightly doped throughout. This $p^+$ bulk in the CMOS process reduces the effective lifetime of the diffusing electrons and thus suppresses the slow current tail and reduces the rise time without any significant reduction in responsivity. An additional advantage of the low-ohmic $p^+$ bulk is the improved isolation between the detectors in a multi-detector circuit, because of the shortened effective diffusion length. Another difference between the processes lies in the existence of the $n^+$ buried layer in the BiCMOS process, which slightly reduces the hole diffusion current and thus the responsivity, and also increases the capacitance as the depletion region is thinner.

Zhou *et al.* (1994) observed and investigated optoelectronic cross-talk with a NMOS transistor and resistor placed close to a pn photodiode which was illuminated with an 830 nm optical signal. They reported that a depleted diode guard ring reduced the crosstalk by ~85% about 30 μm away from the photodiode. This can be used to lower the cross-talk further in multi-detector circuits.

The responses of the photodiodes were simulated in a time-domain with a Matlab program that used continuity equations together with boundary conditions, process parameters and a step-type optical input signal. The measured rise times and responsivities agreed with the simulation results, and thus showed that the simulation works well (paper VII).

An ideal pn photodiode would have a depletion region width of about twice the penetration depth of light, and the layer would be located near the surface of the semiconductor (Sze 1981). In this way the depletion region would efficiently collect nearly all the electron-hole pairs generated and the capacitance of the junction would be small. The width of the depletion region should not be too large, however, as it should not increase the drift time across the junction too much. The responsivity of an ideal pn photodiode is 0.68 A/W at a wavelength of 850 nm, and the penetration depth of the photons is about 18 μm, which calls for a wide depletion region. The depth from the surface of the silicon from which all the minority carriers generated have to be collected in order to achieve a certain responsivity is shown in Fig. 24 as a function of wavelength. In order to achieve 0.5 A/W responsivity at a wavelength of 900 nm, the carriers have to be collected within 40 μm of the surface. The figure also shows that a wavelength of 650 nm would be better, but unfortunately no cheap, powerful pulsed semiconductor lasers are available at that wavelength.

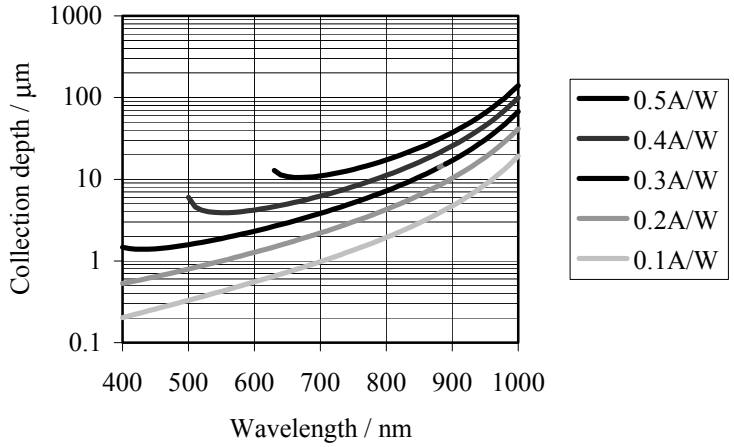


**Fig. 24. Depths within which carriers have to be collected to achieve given responsivities as a function of wavelength.**

The concentrations and depths of junctions cannot be freely adjusted in standard CMOS/BiCMOS processes, and the vertical dimensions are small compared with the penetration depth of the photons at NIR wavelengths. The results of the present work show, however, that a quantum efficiency of about 50% can be achieved even with a response time of a few nanoseconds. In addition, the lower noise partly compensates for the lower responsivity of the photodetector relative to realisations using external PIN photodiodes. The results indicate that photodetectors for a pulsed TOF laser radar module and imaging can be designed using standard CMOS/BiCMOS processes without any process modifications. This could lead to smaller, cheaper and simpler realisations in some applications.

## 3.4 Single chip realisations

An integrated optoelectronic receiver for a pulsed TOF laser radar is presented in paper VIII. The purpose of the circuit is to demonstrate the operation of the receiver with a photodetector integrated into the same chip. The chip includes an integrated pn photodiode (cross-section shown in Fig. 23), a transimpedance preamplifier, a high-pass filter for pulse shaping, current mode gain control, a post-amplifier, a timing comparator and a peak detector, as shown in Fig. 25.

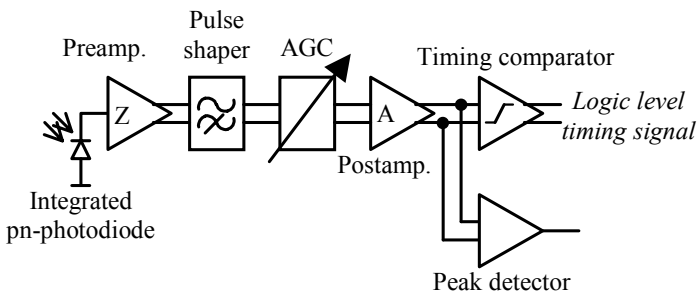


**Fig. 25. Coarse schematic diagram of the integrated receiver channel described in paper VIII.**

The measured bandwidth and maximum transresistance of the amplifier channel are about 150 MHz and 280 kΩ respectively. The input referred noise, 2.1 pA/√Hz, is about three times lower than with the external photodiode realisation described in paper I. This was achieved because of the smaller capacitance of the photodetector and the absence of any parasitic capacitance or inductance of the photodetector and amplifier channel package, PCB wiring, bond wires, I/O cells and ESD protection structures. However, the advantage from the point of view of the minimum usable optical signal is questionable as the responsivity of the integrated photodiode (0.3 A/W) is about a half of that of discrete PIN photodiodes (0.6 A/W) and about 160 times smaller than that of APDs (50 A/W), which in any case present a drawback at a high supply voltage. Nevertheless, the measurements demonstrated that it was possible to integrate the whole receiver channel into a single chip without any process modifications and that the chip could be used for pulsed TOF laser rangefinding.

The performance of the optoelectronic receiver shown in Fig. 25 is summarised in Table 5.

*Table 5. Performance of the receiver for a pulsed TOF laser radar.*

| | |
|---|---|
| bandwidth | ~150 MHz |
| maximum transresistance | 280 kΩ |
| Input-referred current noise | 2.1 pA/√Hz |
| responsivity of the pn photodiode | ~0.3 A/W |
| capacitance of the pn photodiode | 0.54 pF |
| rise time of the pn photodiode | < 5 ns |
| walk error | ±10 ps, (±1.5 mm), (1:30 input signal) |
| single-shot precision | < 200 ps, (< 30 mm), (SNR > 10) |
| current consumption | 20 mA @ 5 V |

Paper IX presents a chip in which the level of integration is further increased by including the time interval measurement. The chip includes four identical optoelectronic receiver channels and a digital-mode three-channel TDC, as shown in Fig. 26. Only optics and a laser pulse transmitter are needed to measure distances in up to three directions with a single optical pulse. The receiver channels consist of an integrated pn photodetector, a transimpedance preamplifier, a high-pass filter for pulse shaping, a post-amplifier, a timing comparator and a peak detector which is common to all the receiver channels.

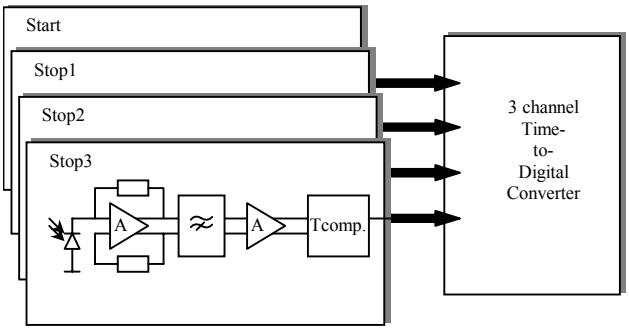


**Fig. 26. Coarse schematic diagram of the multi-channel receiver.**

The chip was designed to demonstrate the feasibility of integrating a whole multi-channel receiver as a single chip in order to measure several distances with a single optical pulse. The photodetectors are circular, with a diameter of 100 μm, and placed in a row. A photograph of the chip is shown in Fig. 27.

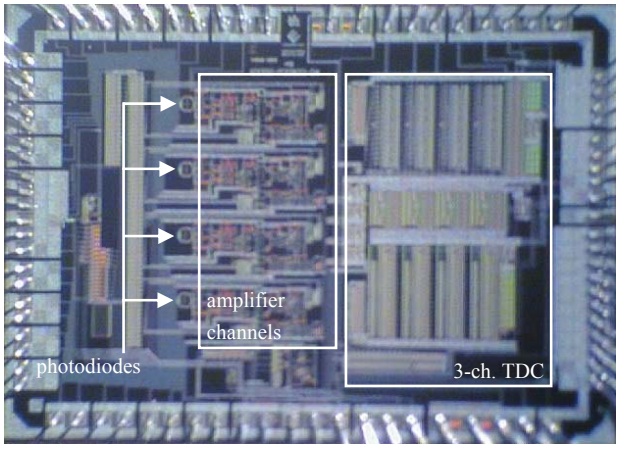


**Fig. 27. Photograph of the multichannel receiver.**

The chip has been implemented in an AMS 0.8 μm BiCMOS process without any process modifications and is 4.6 mm x 3.3 mm in area. The measured bandwidth and transresistance of the amplifier channels are 140 MHz and 390 kΩ respectively and the input-referred noise is 2.2 pA/√Hz. The single-shot precisions are 51 mm and 13 mm with SNRs of 11 and 100.

Since the packaged version of the circuit was unstable because of the inductances of the bond wires and lead frames of the CLCC84 package, the unpackaged chip was bonded directly onto the PCB. A photograph of the chip on the PCB is shown in Fig. 28.

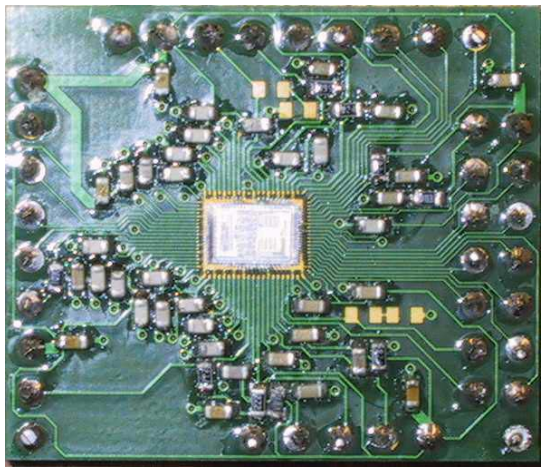

**Fig. 28. A photograph of the hybrid test circuit of the multichannel receiver.**

In the linearity measurements the start channel was used for the start signal and the stop3 channel for the stop signal. Fig. 29 shows a non-linearity of ±12 mm in the range from 0.27 m to 22 m. This non-linearity is caused by cross-talk from the start channel to the stop3 channel, which can be reduced by better design of the preamplifier, which had quite a poor PSRR.

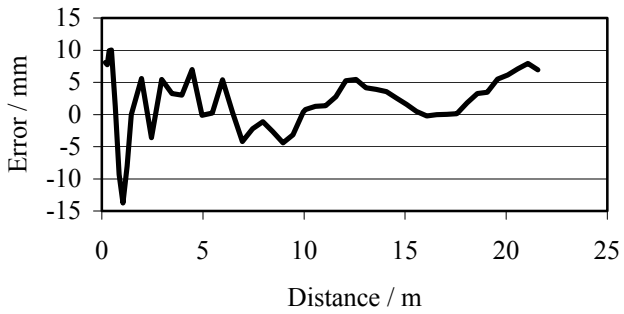


**Fig. 29. Measured linearity error of the multichannel receiver.**

The transmitted optical signal was divided between four fibres for measurement purposes and the reflected signal was focused on the chip. The efficiency of the division was poor and a great deal of power was lost. By designing photodetectors of a customised shape and placing them in a manner appropriate to the application, the efficiency can undoubtedly be improved. Rectangular photodiodes placed next to each other, for example, will effectively collect the signal from a target on which the laser stripe is focused and measure distances from given sectors. Measurements of this kind could be useful in anti-collision warning system for vehicles, for example.

# 4 Discussion

This doctoral thesis reports on the development of electronic and optoelectronic circuits and devices which would be useful for increasing the level of integration of pulsed TOF laser rangefinders and reducing their physical size and complexity. The performance of the innovative features was verified with prototypes of a laser radar module in a real distance measurement environment. The work started with the development of electronics for the receiver channel. Timing discrimination is of great interest in pulsed TOF laser rangefinding, because the measurement is based on the time required for an optical pulse to travel to the target and back and the dynamic range of the input signal level is large. Two types of timing discriminator were developed, a leading edge discriminator in which the signal can saturate in the amplifier channel and a high-pass timing discriminator in which the signal has to be processed linearly and gain control structures are usually used. In addition, a new idea is presented in which the high-pass timing discriminator is combined with analogue time interval measurement.

The leading edge discriminator has a large dynamic range (1:4000), as the signal is allowed to saturate in the receiver, whereas the signal for the high-pass timing discriminator has to be processed linearly. The transimpedance preamplifier usually limits the dynamic range of the signal to about 1:100–1:200, and in this work a current-mode attenuator between the photodetector and the preamplifier and a voltage-mode attenuator between the preamplifier and the postamplifier were used successfully to enlarge the dynamic range up to 1:620. The walk error of the leading edge discriminator after compensation is ±35 mm and that of the high-pass discriminator is ±4 mm. Analysis of the walk error in the leading edge receiver shows that this can be reduced by increasing the bandwidth of the receiver and shortening the rise time of the optical pulse.

Three prototypes for laser rangefinding devices were constructed in order to verify the usability of the receiver channel. The prototypes consumed about a fifth of the power required by earlier realisations which contained discrete components in their receiver channels and achieved similar or even better performance. The prototypes can be used as such for measurement applications involving mm-level accuracy, but serve in particular to show the potential of the new technique with respect to the construction of laser radar modules with a high level of system integration.

Integration of the photodetector into the receiver chip was also investigated by designing and testing several photodetector structures using standard silicon processes. The responsivity of the integrated photodiode (0.3 A/W) is about a half of that of discrete PIN photodiodes at 850–900 nm wavelengths, but the noise of the receiver is lower, because of absence of the parasitic capacitances and inductances caused by packages, PCB wiring, bond wires, the I/O cell and ESD protection structures, and partly compensates for the reduction in the signal. Integration of the photodetector into the receiver chip may be useful in short-range applications, but due to the high internal gain, APD is normally the most attractive alternative, possibly using hybrid realisation, although the latter would increase the number of components, as a high voltage has to be generated for the APD.

Finally, the operation of the integrated imaging TOF laser radar was demonstrated with a chip which can be used to measure distances in three directions with a single laser pulse. The chip includes four photodetectors and receiver channels to produce logic-level timing signals and a three-channel time-to-digital converter. The optics and the laser pulse transmitter are external components in the system.

In some applications a visible measurement beam helps to set up the measurement, and an additional visible pointer beam or an IR viewer is essential when using infrared lasers. This envoked the idea of using visible lasers as pulse sources. CW lasers developed for DVD-RAM purposes with a wavelength of about 650 nm are currently available that achieve an optical power of 50 mW. This power is very low relative to the high-power infrared pulse lasers used in this work (~100 W), but it is enough for short-range applications (up to 10 metres) or for applications in which reflectors can be used as targets (Banner). The driving electronics of the CW laser diode can be constructed with a supply of a few volts, which is advantageous, as the drivers of high-power pulsed lasers needs hundreds of volts in order to achieve pulse widths below 10 nanoseconds.

There are only a few papers in the literature concerned with transimpedance preamplifiers in which measurements are performed with a photodiode capacitance comparable to that available here. Phang *et al.* (1999) reported a preamplifier implemented in a 0.35 μm CMOS process which also employed fully differential structure in connection with the external photodiode generating the input to it. The circuit achieved a transresistance of 19 kΩ, a bandwidth of 70 MHz and an input-referred noise of 6.7 pA/√Hz with a photodiode capacitance of 5 pF. The same group described in Zand *et al.* (2001) an improved version of the preamplifier in which a common gate input was used to isolate the capacitance of the external photodiode. This preamplifier was also implemented in a 0.35 μm CMOS process and achieved a transresistance of 33 kΩ, a bandwidth of 255 MHz and an input-referred noise of 6.8 pA/√Hz with a photodiode capacitance of 2 pF. Pennala *et al.* (2000) reported a receiver channel implemented using a MAXIM GST-2 semi-custom bipolar ($f_T$=27 GHz) array that achieved a bandwidth of 1 GHz, a transresistance of 11 kΩ and an input-referred noise of 10 pA/√Hz with a photodiode capacitance of 1.5 pF. The performance of the transimpedance preamplifiers described to date is summarised in Table 6.

*Table 6. Comparison of transimpedance amplifier channels.*

| $I_n$ [pA/√Hz] | $C_{pd}$ [pF] | BW [MHz] | $R_T$ [kΩ] | Process | Reference |
|---|---|---|---|---|---|
| 6 | 2 | 170 | 260 | 0.8 BiCMOS | Paper I |
| 6.7 | 5 | 70 | 19 | 0.35 CMOS | Phang *et al.* 1999 |
| 6.8 | 2 | 255 | 33 | 0.35 CMOS | Zand *et al.* 2001 |
| 10 | 1.5 | 1000 | 11 | MAXIM GST-2 | Pennala *et al.* 2000 |

In the field of timing discriminators, Ruotsalainen *et al.* (1995b) reported a ±60 ps walk error in a dynamic range of 1:4.4 in a 1.2 µm CMOS process and a ±30 ps walk error in a range of 1:70 in a 1.2 µm BiCMOS process. Both circuits employed a high-pass timing discriminator and walk error compensation with an offset voltage, and the pulse had a rise time of ~1 ns, a half-value width of ~7 ns and a fall time of ~2.5 ns. Jackson *et al.* (1997) reported a ±150 ps walk error in a range of 1:100 using a lumped-element R-C for shaping the pulse in a CFD. The chip was implemented in a 1.2 µm CMOS process and the rise and fall times of the pulse were ~5 ns and ~15 ns. Simpson *et al.* (1997) reported a ±250 ps walk error in a range of 1:100 using a high-pass timing discriminator implemented in a 1.2 µm CMOS process. The rise and fall times of the pulse were 10 ns. Pennala *et al.* (2000) reported a ±20 ps walk error in a range of 1:17. The chip was implemented in a MAXIM GST-2 technology semi-custom bipolar array and the rise time and width of the optical pulse were ~40 ps and ~80 ps respectively. The detection method was high-pass timing discrimination together with walk compensation by means of an offset voltage. The combination of the high-pass timing discriminator and time-to-amplitude conversion presented in paper III achieves a ±3.5 walk error in a range of 1:21. The performance of the timing discriminators is summarised in Table 7.

*Table 7. Comparison of timing discriminators.*

| Discr. | Walk error [ps] | Dynamic range | Process | Reference |
|---|---|---|---|---|
| High-pass | ±60 | 1:4.4 | 1.2 CMOS | Ruotsalainen *et al.* 1995b |
| CFD, R-C | ±150 | 1:100 | 1.2 CMOS | Jackson *et al.* 1997 |
| High-pass | ±250 | 1:100 | 1.2 CMOS | Simpson *et al.* 1997 |
| High-pass | ±30 | 1:70 | 1.2 BiCMOS | Ruotsalainen *et al.* 1995b |
| High-pass | ±12 | 1:10 | 0.8 BiCMOS | Paper I |
| High-pass | ±20 | 1:17 | MAXIM GST-2 | Pennala *et al.* 2000 |
| HP/TAC | ±3.5 | 1:21 | 0.8 BiCMOS | Paper III |

To the best of the author's knowledge, no papers have yet been presented in the field of imaging devices utilising a focal plane array and the pulsed time-of-flight measurement principle. Lange & Seitz (2001) described a 3-D time-of-flight camera with 64 x 25 pixels that employs a focal plane array, but the measurement is based on continuous wave (CW) modulation. The unambiguous distance range is 7.5 metres and the chip can measure 10 frames per second with an accuracy of less than 5 cm.

In conclusion, this thesis describes high performance circuits for pulsed time-of-flight laser rangefinding and high performance laser radar modules developed especially for industrial applications. The results pave the way to a component-like laser radar construction which would certainly increase the number of applications for such a

technology. Moreover, the laser radar chip, including customised photodetectors with receiver channels and multi-channel time interval measurement circuitry, has been shown to be successfully implementable using current semiconductor processes.

# 5 Summary

The general objective of the work was to increase the level of integration of pulsed time-of-flight laser radar devices. One specific aim was to construct a laser radar module which can be used for different measurement tasks by means of an external fibre-connected measurement head customised for the application. Another purpose of the module construction was to verify the functionality of the receiver ASICs developed here, which are necessary when increasing the integration level of the system. The ultimate goal of the work was to pave the way to a single-chip realisation which would include parallel customised photodetectors with receiver channels and a multi-channel TDC.

Three receiver channels were developed: one with a leading edge discriminator that achieves a compensated walk error of ±35 mm in an input signal dynamic range of 1:4000, one with a high-pass timing discriminator that achieves a walk error of ±4 mm with an input signal dynamic range of 1:620 and one in which the high-pass timing discriminator is combined with time-to-amplitude conversion that achieves a walk error of ±0.5 mm with an input signal dynamic range of 1:21. The level of integration is highest in the latter receiver, as time interval measurement is located in the same chip.

The usability of the receiver channels was verified by constructing laser radar modules which can be also used as such for measurement purposes. The device achieves mm-level measurement accuracy with passive targets over a range from 4 to 34 metres. The measurement range can be modified for each application by designing a customised optomechanical measurement head. The laser radar technology developed here can be used for a wide variety of measurements, including positioning of tools and vehicles, velocity measurement, anti-collision radars and proximity sensors, for example.

Integration of the photodetector into the same chip as the rest of the receiver channel electronics was also addressed. The responsivity of the photodiode is about 0.3 A/W, but the noise level of the receiver is reduced by a factor of about three because of the absence of parasitic capacitances and inductances caused by photodiode and receiver channel packages, PCB wiring, bond wires, the I/O cell and ESD protection structures. The receiver structure can be multiplied, as was demonstrated by designing and testing a laser radar chip which includes four receiver channels with photodiodes and a three-channel time-to-digital converter that can be used to measure distances in three directions with a

single optical pulse. The laser pulse transmitter and the optics are external components of the system.

The scientific contribution of this work, in the addition to the circuits and devices that were developed, lies in the analysis of walk error in the leading edge discriminator, which proves the significance of the receiver bandwidth and rise time of the optical pulse, the totally new receiver channel structure combining timing discrimination with time interval measurement and the demonstration of a laser radar chip which includes four receiver channels with photodiodes and a three-channel time-to-digital converter. All of these contributions improve the level of integration of the pulsed time-of-flight laser rangefinding module.

# References


Ahola R (1979) Design of the transmitter and receiver of a laser rangefinder system for moving targets. (Liikkuvan kohteen Laser-etäisyysmittauslaitteiston lähettimen ja vastaanottimen suunnittelu). Dipl. Eng. thesis, University of Oulu, Department of Electrical Engineering.

Ahola R (1987) A pulsed time-of-flight laser rangefinder for fast, short-range, high resolution applications. Acta Univ Oul C 38.

Araki T & Yoshida H (1996) Optical distance meter using a pulsed laser diode and fast avalanche photo diodes for measurement of molten steel levels. Transactions of the ASME 118:800-803.

Banner (2002) L-gage LT3, Long-Range Time-of-Flight Laser Distance-Gauging Sensors. Banner Engineering Corp., Minneapolis, U.S.A.

Bertolini G (1968) Pulse shape and time resolution. In: Bertolini G & Coche A (eds) Semiconductor Detectors. North-Holland Publishing, Amsterdam, Holland.

Biber A, Seitz P & Jäckel H (2001) Avalanche photodiode image sensor in standard silicon BiCMOS technology. Sensors and Actuators A 2885: 1-7.

Binkley DM & Casey ME (1988) Performance of fast monolithic ECL voltage comparators in constant-fraction discriminators and other timing circuits. IEEE Transactions on Nuclear Science 35(1): 226-230.

Cherry EM & Hooper DE (1963) The design of wide-band transistor feedback amplifiers. Proceedings I.E.E, 110(2): 375-389.

Gedcke DA & McDonald WJ (1968) Design of the constant fraction of pulse height trigger for optimum time resolution. Nuclear Instruments and Methods 58: 253-260.

Ghioni M, Zappa F, Kesan VP & Warnock J (1996) A VLSI-compatible high-speed silicon photodetector for optical data link applications. IEEE Transactions on Electron Devices 43(7): 1054-1060.

Gilbert B (1968) A precise four-quadrant multiplier with subnanosecond response. IEEE Journal of Solid-State Circuits 3(4): 365-373.

Hewlett-Packard Inc. Time interval averaging. Application note 162-1.

IEEE (1996) The IEEE Standard Dictionary of Electrical and Electronics Terms. IEEE Standard 100-1996. IEEE Standards Office, Piscataway, New Jersey, USA.

Jackson RG, Blalock TV, Simpson ML, Wintenberg AL & Young GR (1997) Integrated constant-fraction discriminator shaping techniques for the PHENIX lead-scintillator calorimeter. IEEE Transactions on Nuclear Science 44(3): 303-307.

Kaisto I, Kostamovaara J, Manninen M & Myllylä R (1993) Laser radar based measuring system for large scale assembly applications. Proc. SPIE International Conference on Laser Dimensional Metrology: Recent Advances for Industrial Application, Brighton, United Kingdom, 2088: 121-130.

Kawashima S, Watanabe K & Kobayashi K (1995) Traffic condition monitoring by laser radar for advanced safety driving. Proc. of the Intelligent Vehicles ‘95 Symposium, Detroit, USA, 299-303.

Kinbara S & Kumahara T (1969) A leading-edge time pickoff circuit. Nuclear Instruments and Methods 69: 261-266.

Kostamovaara J & Myllylä R (1985) A time-to-amplitude converter with constant fraction timing discriminators for short time interval measuring. Nuclear Instruments and Methods in Physics Research A239: 568-578.

Kostamovaara J (1986) Techniques and devices for positron lifetime measurement and time-of-flight laser rangefinding. Acta Univ Oul C 37.

Kyomasu M (1995) Development of an integrated high speed silicon PIN photodiode sensor. IEEE Transactions on Electron Devices 42(6): 1093-1099.

Lange R & Seitz P (2001) Solid-state time-of-flight range camera. IEEE Journal of Quantum Electronics 37(3): 390-397.

Lim PJW, Tzeng AYC, Chuang HL & Onge SAS (1993) A 3.3-V monolithic photodetector/CMOS preamplifier for 531 Mb/s optical data link applications. Proc. IEEE International Solid-State Circuits Conference, ISSCC’93 : 96-97.

Myllylä R, Marszalec J, Kostamovaara J, Mäntyniemi A & Ulbrich G-J (1998) Imaging distance measurements using TOF lidar. Journal of Optics 29(3): 188-193.

Määttä K, Kostamovaara J & Myllylä R (1990) On the measurement of hot surfaces by pulsed time-of-flight laser radar techniques. Proc. SPIE International Congress on Optical Science and Engineering: Industrial Inspection II, Hague, Netherlands, 1265: 179-191.

Määttä K, Kostamovaara J & Myllylä R (1993) Profiling of hot surfaces by pulsed time-of-flight laser range finder techniques. Applied Optics 32(27): 5334-5347.

Määttä K & Kostamovaara J (1997) Accurate liquid level gauge based on pulsed time-of-flight principle. SPIE Proceeding 3100: 268-277.

Määttä K (1995) Pulsed time-of-flight laser rangefinding techniques and devices for hot surface profiling and other industrial applications. Acta Univ Oul C 81.

Palojärvi P, Ruotsalainen T & Kostamovaara J (1997) A variable gain transimpedance amplifier channel with a timing discriminator for a time-of-flight laser radar. Proc. IEEE European Solid-State Circuits Conference, ESSCIRC'97 : 384-387.

Paulus TJ (1985) Timing electronics and fast timing methods with scintillation detectors. IEEE Transactions on Nuclear Science NS-32(3): 1242-1249.

Pennala R, Kilpelä A & Kostamovaara J (2000) An integrated receiver channel for picosecond range laser radar pulses. Proc. 43rd IEEE Midwest Symposium on Circuits and Systems, MWSCAS’00 : 702-705.

Phang K & Johns DA (1999) A CMOS optical preamplifier for wireless infrared communications. IEEE Transactions on Circuits and Systems II: Analog and Digital Signal Processing 46(7): 852-859.

Ruotsalainen T, Palojärvi P & Kostamovaara J (1995a) A 160 MHz BiCMOS differential amplifier channel with gain control for the receiver of a portable laser rangefinding device. Proc. 38th Midwest Symposium on Circuits and Systems, MWSCAS’95 : 1030-1033.

Ruotsalainen T, Palojärvi P & Kostamovaara J (1995b) BiCMOS and CMOS timing detectors for the receiver of a portable laser rangefinding device. Proc. 38th Midwest Symposium on Circuits and Systems, MWSCAS’95 : 1022-1025.

Ruotsalainen T (1999a) Integrated receiver channel circuits and structures for a pulsed time-of-flight laser radar. Acta Univ Oul C 136.

Ruotsalainen T, Palojärvi P & Kostamovaara J (1999b) A current-mode gain control scheme with constant bandwidth and propagation delay for a transimpedance preamplifier. IEEE Journal of Solid-State Circuits 34(2): 253-258.

Räisänen-Ruotsalainen E, Rahkonen T & Kostamovaara J (1995) A low-power CMOS time-to-digital converter. IEEE Journal of Solid-State Circuits 30(9): 984-990.

Räisänen-Ruotsalainen E (1998) Integrated time-to-digital converter implementations. Acta Univ Oul C 122.

Räisänen-Ruotsalainen E, Rahkonen T & Kostamovaara J (2000) An integrated time-to-digital converter with 30-ps single-shot precision. IEEE Journal of Solid-State Circuits 35(10): 1507-1510.

Samuels M, Patterson S, Eppstein J & Fowler R (1992) Low cost, handheld lidar system for automotive speed detection and law enforcement. Proc. SPIE International Conference on Laser Radar VII: Advanced Technology for Applications, Los Angeles, California, USA, 1633: 147-159.

Simpson ML, Britton CL, Wintenberg AL & Young GR (1997) An integrated CMOS time interval measurement system with subnanosecond resolution for the WA-98 calorimeter. IEEE Journal of Solid-State Circuits 32(2): 198-205.

Simpson ML & Paulus MJ (1998) Discriminator design considerations for time-interval measurement circuits in collider detector systems. IEEE Transactions on Nuclear Science 45(1): 98-104.

Schow CL, Schaub JD, Li R, Qi J & Campbell JC (1999) A monolithically integrated 1-Gb/s silicon photoreceiver. IEEE Photonics Technology Letters 11(1): 120-121.

Sze S (1981) Physics of Semiconductor Devices. John Wiley & Sons, New York, USA.

van de Plassche R (1994) Integrated Analog-to-Digital and Digital-to-Analog Converters. Kluwer Academic Publishers, Netherlands.

Vanisri T & Toumazou C (1995) Integrated high frequency low-noise current-mode optical transimpedance preamplifiers: theory and practice. IEEE Journal of Solid-State Circuits 30(6): 677-685.

Wieland J, Duran H & Felder A (1994) Two-channel 5 Gbit/s silicon bipolar monolithic receiver for parallel optical interconnects. Electronics Letters 30(4): 358-359.

Woodward TK & Krishnamoorthy (1998) 1 Gbit/s CMOS photoreceiver with integrated detector operating at 850nm. Electronics Letters 34(12): 1252-1253.

Yahya CB (2000) Design of wideband low noise transimpedance amplifiers for optical communication. Proc. 43rd IEEE Midwest Symposium on Circuits and Systems, MWSCAS'00 : 804-807.

Yamamoto M, Kubo M & Nakao K (1995) Si-OEIC with a built-in pin-photodiode. IEEE Transactions on Electron Devices 42(1): 58-63.

Zand B, Phang K & Johns DA (2001) A transimpedance amplifier with DC-coupled differential photodiode current sensing for wireless optical communication. Proc. IEEE 2001 Custom Integrated Circuits Conference: 455-458.

Zhou MJ, Holleman J & Wallinga H (1994) Elimination or minimisation of optoelectronic crosstalk between photodiodes and electronic devices in OEIC on Si. Electronics Letters 30(11): 895-897.

Ziemer R & Tranter W (1985) Principles of Communications. 2nd ed., Houghton Mifflin, Boston, USA.

Zimmermann H (1996) Monolithic bipolar-, CMOS-, and BiCMOS-receiver OEICs. Proc. Int. Semicond. Conference, CAS'96, Sinaia, Romania: 31-40.